Geometric analysis of oscillations in the Frzilator model

Taghvafard, Hadi; Jardon Kojakhmetov, Hildeberto; Szmolyan, Peter; Cao, Ming

Published in:
Journal of Mathematical Analysis and Applications

DOI:
10.1016/j.jmaa.2020.124725

Publication date:
2021

J. Math. Anal. Appl. 495 (2021) 124725

Contents lists available at ScienceDirect

Journal of Mathematical Analysis and Applications

www.elsevier.com/locate/jmaa

Geometric analysis of oscillations in the Frzilator model

Hadi Taghvafard [a,*,1,2], Hildeberto Jardón-Kojakhmetov [b,3], Peter Szmolyan [c,4], Ming Cao [a,2]

[a] *Engineering and Technology Institute, Faculty of Science and Engineering, University of Groningen, 9747 AG Groningen, the Netherlands*
[b] *Faculty of Science and Engineering, Bernoulli Institute, University of Groningen, 9747 AG, Groningen, the Netherlands*
[c] *Institute for Analysis and Scientific Computing, Technische Universität Wien, 1040 Wien, Austria*

ARTICLE INFO

Article history:
Received 2 December 2019
Available online 27 October 2020
Submitted by S.A. Fulling

Keywords:
Slow-fast system
Relaxation oscillations
Blow-up method
Geometric singular perturbation theory
Myxobacteria

ABSTRACT

A biochemical oscillator model, describing developmental stage of myxobacteria, is analyzed mathematically. Observations from numerical simulations show that in a certain range of parameters, the corresponding system of ordinary differential equations displays stable and robust oscillations. In this work, we use geometric singular perturbation theory and blow-up method to prove the existence of a strongly attracting limit cycle. This cycle corresponds to a relaxation oscillation of an auxiliary system, whose singular perturbation nature originates from the small Michaelis-Menten constants of the biochemical model. In addition, we give a detailed description of the structure of the limit cycle, and the timescales along it.

1. Introduction

Oscillators are ubiquitous in different fields of science such as biology [33], biochemistry [8,11], neuroscience [15], medicine [12,30,29], and engineering [31]. In particular, biochemical oscillations often occur in several contexts including signaling, metabolism, development, and regulation of important physiological cell functions [25]. In this paper, we study a biochemical oscillator model that describes the developmental stage of *myxcobacteria*. Myxcobacteria is multicellular organisms that are common in the topsoil [3]. During vegetation growth, i.e. when food is ample, myxobacteria constitute small swarms by a mechanism called

* Corresponding author.
E-mail address: taghvafard@gmail.com (H. Taghvafard).
[1] Current address: Division of Systems Biomedicine and Pharmacology, Leiden Academic Center for Drug Research, Leiden University, Leiden, the Netherlands.
[2] The work of H. Taghvafard and M. Cao was supported in part by the European Research Council (ERC-CoG-771687) and the Netherlands Organisation for Scientific Research (NWO-vidi-14134).
[3] H. Jardón-Kojakhmetov was supported by the Alexander von Humboldt Foundation.
[4] The research of P. Szmolyan was funded by WWTF under the grant MA14-049.

https://doi.org/10.1016/j.jmaa.2020.124725
0022-247X/

"gliding" [16]. In contrast, under a starvation condition, they aggregate and initiate a complex developmental cycle during which small swarms are transformed into a multicellular single body known as "fruiting body", whose role is to produce spores for next generation of bacteria [3]. During the aforementioned transition, myxobacteria pass through a developmental stage called the "ripple phase" [16,3], characterized by complex patterns of waves that propagate within the whole colony.

Two genetically distinct molecular motors are concentrated at the cell poles of myxobacteria, allowing them to glide on surfaces; these two motors are called Adventurous (A-motility) and Social (S-motility) motors, respectively [16]. The role of the former is to push the cells forward, while the role of the latter is to pull them together. So, in order for a cell to reverse its direction, it has to alternatively activate its A-motility (push) and S-motility (pull) motors at opposite cell poles [16]. As a result, by forward and backward motion of myxobacteria, complex spatial wave patterns are created. In particular, wave patterns are produced by the coordination of motion of individual cells through a direct end-to-end contact signal, the "C-signal". During the ripple phase of development, the C-signaling induces reversals, while suppresses them during the aggregation stage of development. Observations from experiments resulted in proposing a biochemical oscillator in [16], known as the Frzilator, which acts as a "clock" to control reversals.

The Frzilator is detailed in Section 2.1. From our numerical simulations, it appears that this biochemical oscillator is robust under small variation of parameters. More importantly, it seems that (almost) all solutions converge to a "unique" limit cycle. Regarding the previous property, in [28] it has been shown that within a certain range of parameter values, (almost) all trajectories are oscillatory, the system has a finite number of isolated periodic orbits, at least one of which is asymptotically stable. Although some biological systems may produce more than one stable periodic solution for a certain range of parameters [4], the coexistence between multiple stable solutions has not yet been observed *experimentally* [9].

The main contribution of this paper is to prove that, within a certain range of parameter values, there exists a *strongly attracting* periodic orbit for the Frzilator. Moreover, the detailed description of the structure of such periodic orbit is given. The methodology used to prove the aforementioned result consists first on an appropriate rescaling of the original model, which leads to a slow-fast (or two timescales) system; next, we take advantage of the two timescales of the rescaled system to develop a geometric analysis via techniques of multi-timescale dynamical systems. From the multi-timescale nature of the problem, it turns out that the limit cycle is in fact a relaxation oscillator, meaning that there are several timescales along the orbit of the oscillator. From an analytical point of view, the main difficulty of this analysis is the detailed description of a transition along two non-hyperbolic lines (see details in Section 3). Our analysis is based on the approach developed in [18,19] where similar mechanisms, leading to an attracting limit cycle in the Goldbeter minimal model [8], have been studied. The C-signal of the biological oscillator plays a crucial role both in our analysis and in the behavior of the limit cycle. Thus, besides proving the existence of a strongly attracting limit cycle using geometric singular perturbation theory and blow-up method, we have performed a two-parameter bifurcation analysis to show which combination of the C-signal and Michaelis-Menten constants of the system leads to oscillatory motions. In addition, we have computed a certain range for γ over which our main result is valid.

The rest of this paper is organized as follows. In Section 2 we introduce the model, perform some preliminary analysis on the model, and briefly introduce the tools which we are going to use in the paper. In Section 3 we give the slow-fast analysis of an auxiliary system, corresponding to the original system. More precisely, we discuss the behavior of the dynamics when $\varepsilon \to 0$. In Section 4, we present the blow-up analysis of the non-hyperbolic parts. We conclude the paper with a discussion and outlook in Section 5.

2. Detailed model and preliminary analysis

In this section we provide a preliminary analysis of the biochemical oscillator proposed in [16]. We start in Subsection 2.1 by presenting a detailed description of the model under study. Furthermore, we describe

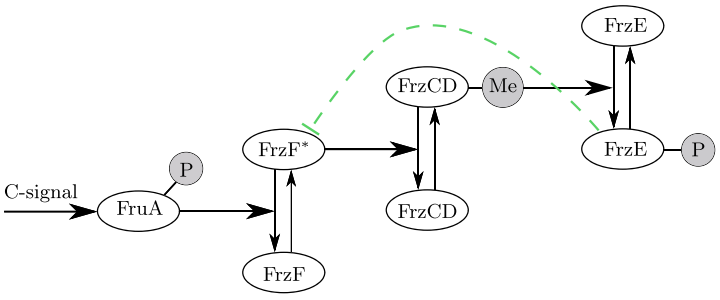

Fig. 1. Essential components of the Frzilator.

the behavior of the trajectories and the role of parameters, and propose a unification of them. Afterwards, in Subsection 2.2, we present a two-parameter bifurcation analysis where we clarify the nature and the role of two distinct parameters of the system. Finally, in Subsection 2.3 we provide a brief introduction to slow-fast systems and the main techniques for their analysis.

2.1. Model description

We study a biochemical oscillator model which describes the social-behavior transition phase of myxobacteria [16]. This model, which is known as the Frzilator (or simply "Frz") model, is based on a negative feedback loop. In the Frz model, there are three proteins, namely, a methyltransferase (FrzF), the cytoplasmic methyl-accepting protein (FrzCD), and a protein kinase (FrzE). A direct and end-to-end collision of two myxobacteria results in producing a signal, so-called "C-signal", under which a protein called FruA is phosphorylated. The signal from phosphorylated FruA (FruA-P) activates the Frz proteins as follows [16]: (i) the methyltransferase FrzF (FrzF*) is activated by the protein FruA-P; (ii) in response to FrzF*, the protein FrzCD is methylated (FrzCD-M); (iii) the phosphorylation of FrzE (FrzE-P) is activated by the methylated form of FrzCD; (iv) FrzF* is inhibited by the phosphorylated form of FrzE. Fig. 1 shows a schematic representation of interactions between proteins of the Frz system. For a more detailed explanation of the model and its biological background, see [16]. Denote f, c and e respectively as the fraction of activated FrzF, methylated FrzCD, and phosphorylated FrzE. These fractions are given by [16]

$$f = \frac{[\text{FrzF}^*]}{[\text{FrzF}^*] + [\text{FrzF}]}, \qquad c = \frac{[\text{FrzCD-M}]}{[\text{FrzCD}] + [\text{FrzCD-M}]}, \qquad e = \frac{[\text{FrzE-P}]}{[\text{FrzE}] + [\text{FrzE-P}]}.$$

The interaction between the Frz proteins is modeled by Michaelis-Menten kinetics and hence leads to the dynamical system

$$\begin{aligned} \frac{df}{d\tau} &= k_{\text{a}}(1-f) - k_{\text{d}} f e, \\ \frac{dc}{d\tau} &= k_{\text{m}}(1-c) f - k_{\text{dm}} c, \\ \frac{de}{d\tau} &= k_{\text{p}}(1-e) c - k_{\text{dp}} e, \end{aligned} \tag{1}$$

where

$$
\begin{aligned}
k_{\mathrm{a}} &= \frac{k_{\mathrm{a}}^{\max}}{K_{\mathrm{a}} + (1-f)}, \qquad & k_{\mathrm{d}} &= \frac{k_{\mathrm{d}}^{\max}}{K_{\mathrm{d}} + f},\\
k_{\mathrm{m}} &= \frac{k_{\mathrm{m}}^{\max}}{K_{\mathrm{m}} + (1-c)}, \qquad & k_{\mathrm{dm}} &= \frac{k_{\mathrm{dm}}^{\max}}{K_{\mathrm{dm}} + c},\\
k_{\mathrm{p}} &= \frac{k_{\mathrm{p}}^{\max}}{K_{\mathrm{p}} + (1-e)}, \qquad & k_{\mathrm{dp}} &= \frac{k_{\mathrm{dp}}^{\max}}{K_{\mathrm{dp}} + e}.
\end{aligned} \tag{2}
$$

Remark 1. Due to the fact that f, c and e represent fractions of active protein concentrations, their values are restricted to $[0,1]$. So the fraction of inactive protein concentrations are given by $(1-f)$, $(1-c)$ and $(1-e)$. Therefore, hereafter, our analysis is restricted to the unit cube

$$
\mathcal{Q} = \left\{ (f,c,e) \in \mathbb{R}^3 \,|\, f \in [0,1],\, c \in [0,1],\, e \in [0,1] \right\}. \tag{3}
$$

As mentioned in [16], the Frz system has the well-known property of "zero-order ultrasensitivity" which requires that the Michaelis-Menten constants $K_{\mathrm{a}}, K_{\mathrm{d}}, K_{\mathrm{m}}, K_{\mathrm{dm}}, K_{\mathrm{p}}$ and K_{dp} have to be *small* [10]. It is observed *numerically* in [16] that for the parameter values $K_{\mathrm{a}} = 10^{-2}$, $K_{\mathrm{d}} = K_{\mathrm{m}} = K_{\mathrm{dm}} = K_{\mathrm{p}} = K_{\mathrm{dp}} = 5 \times 10^{-3}$, $k_{\mathrm{d}}^{\max} = 1\ \mathrm{min}^{-1}$, $k_{\mathrm{m}}^{\max} = k_{\mathrm{p}}^{\max} = 4\ \mathrm{min}^{-1}$, $k_{\mathrm{dm}}^{\max} = k_{\mathrm{dp}}^{\max} = 2\ \mathrm{min}^{-1}$, and $k_{\mathrm{a}}^{\max} = 0.08\ \mathrm{min}^{-1}$, system (1) has an attracting periodic solution. Owing to the fact that the unit of $k_{\mathrm{d}}^{\max}$, $k_{\mathrm{m}}^{\max}$, $k_{\mathrm{p}}^{\max}$, $k_{\mathrm{dm}}^{\max}$ and $k_{\mathrm{dp}}^{\max}$ is min^{-1}, to make the model non-dimensional, we divide all equations of system (1) by $k_{\mathrm{d}}^{\max}$. Note that this does not change the qualitative behavior of the system, while makes all its parameters dimensionless. For simplicity, we unify all the dimensionless Michaelis-Menten constants by $K_{\mathrm{a}} = 2K_{\mathrm{d}} = 2K_{\mathrm{m}} = 2K_{\mathrm{dm}} = 2K_{\mathrm{p}} = 2K_{\mathrm{dp}} = \varepsilon \ll 1$. After unifying all Michaelis-Menten constants by ε, denoting $\gamma := k_{\mathrm{a}}^{\max}$, and substituting (2) in (1), we obtain the following dynamical system

$$
\begin{aligned}
\frac{df}{d\tau} &= \frac{\gamma(1-f)}{\varepsilon + (1-f)} - \frac{2fe}{\varepsilon + 2f},\\
\frac{dc}{d\tau} &= \frac{8(1-c)f}{\varepsilon + 2(1-c)} - \frac{4c}{\varepsilon + 2c},\\
\frac{de}{d\tau} &= \frac{8(1-e)c}{\varepsilon + 2(1-e)} - \frac{4e}{\varepsilon + 2e}.
\end{aligned} \tag{4}
$$

Figs. 2 and 3 show numerically computed attracting limit cycle as well as time evolution of system (4) for $\varepsilon = 10^{-3}$ and $\gamma = 0.08$.

Remark 2. For our analysis in this paper, we fix $\gamma = 0.08$, while later we show that this parameter can be relaxed to some extent, see Remark 3 and Appendix A.

The dynamics along the limit cycle, shown in Fig. 2, can be summarized as follows. Initially, all protein ratios f, c and e are close to zero, under the dynamics (4), the variable f increases (due to the action of the C-signal), while c and e stay close to zero. Once the variable f passes the activation threshold $f^* := 0.5$, the variable c increases very fast. Next, once the variable c passes the threshold $c^* := 0.5$, the variable e is activated and also increases very fast until it reaches its maximum value, i.e., $e = 1$. Due to the fact that there is a negative feedback from e to f, the increase in e results in the degradation of variable f. Once f reaches the threshold f^*, variable c decreases, and once c reaches the threshold c^*, the variable e decreases vary fast. As a result, the variables f and c reach their lowest values (i.e. very close to zero), but the variable e reaches the threshold $e^* := \gamma$. Once the variable e drops below the threshold e^*, the variable f is activated and increases. This behavior is repeated in a periodic manner and a limit cycle is formed (see Fig. 2).

For system (4), a parameter-robustness analysis with respect to ε and $\gamma = 0.08$ is presented in [28]. More precisely, using bifurcation analysis, it is shown that system (4) is robust under the variation of ε for

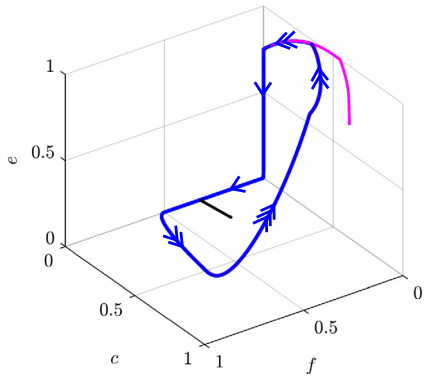

Fig. 2. Numerically computed attracting limit cycle of system (1) for $\varepsilon = 10^{-3}$ and $\gamma = 0.08$. The arrows indicate the direction and speed of the flow along the limit cycle. A single arrow corresponds to the slowest time scale, while three arrows indicate the fastest one.

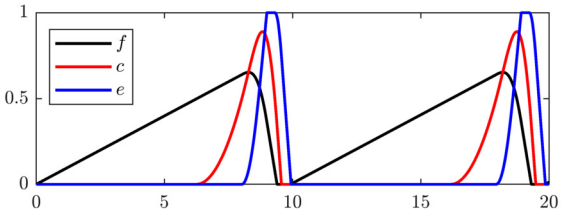

Fig. 3. Numerically computed periodic solution of system (1) for $\varepsilon = 10^{-3}$ and $\gamma = 0.08$.

$\varepsilon \in (0, \varepsilon^*)$ with $\varepsilon^* := 0.05517665$. Moreover, it is proven that for $\varepsilon \in (0, \varepsilon^*)$, almost all trajectories converge to a *finite* number of periodic solutions, one of which is orbitally asymptotically stable. In this article, we prove the existence of a strongly attracting limit cycle which explains the numerically computed periodic orbit, for sufficiently small $\varepsilon > 0$.

2.2. Two-parameter bifurcation analysis

This section is devoted to the two-parameter bifurcation analysis of (4). In particular, we are interested in understanding the behavior of system (4) under the variation of parameters (ε, γ). To this end, let us represent (4) by

$$\dot{x} = G(x; \varepsilon, \gamma), \tag{5}$$

where $x = [f \quad c \quad e]^\top$, and $G(x; \varepsilon, \gamma)$ denotes the right-hand side of (4). We have used the numerical continuation software MATCONT [5] to compute the two-parameter bifurcation diagram of (5) with respect to (ε, γ), presented in Fig. 4, where the vertical and the horizontal axes show, respectively, the behavior of $G(x; \varepsilon, \gamma)$ with respect to ε and γ. The blue curve indicates that for any $0 < \gamma < 1$ and any ε below the curve, the system has unstable equilibria. Owing to the fact that system (4) is cyclic [28, Theorem 5.7], according to [28, Theorems 5.5 & 5.7] almost all trajectories of system (4) converge to a limit cycle for any $0 < \gamma < 1$ and any ε below the bifurcation curve, depicted in Fig. 4. For those values of ε which are above the blue curve, the system is not oscillatory anymore, i.e. the equilibrium point is stable. In fact, the blue curve is a curve of Hopf bifurcations where the equilibria of the system switches from being stable to unstable: with fixed $0 < \gamma < 1$, as ε passes through the curve from above to below, a limit cycle is generated.

As shown in Fig. 4, there are two points, denoted by "GH", which are generalized Hopf (or Bautin) Bifurcation points. At these points, the equilibria of (5) have a pair of purely imaginary eigenvalues at which

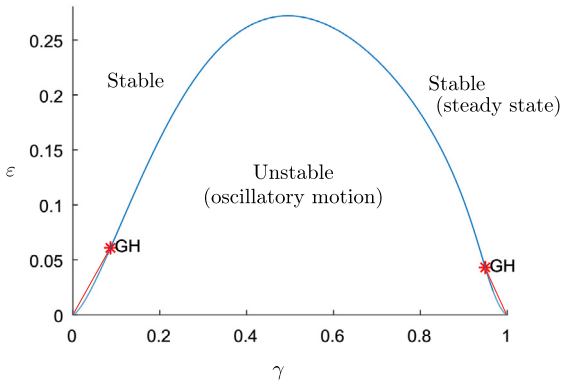

Fig. 4. Two-parameter bifurcation analysis of (4) with respect to (ε, γ). (For interpretation of the colors in the figure(s), the reader is referred to the web version of this article.)

the first Lyapunov exponent coefficient of the Hopf bifurcation vanishes [23]. Computed by MATCONT, the values of (ε, γ) at "GH" points are as follows:

$$(\varepsilon_1, \gamma_1) = (0.060907128, 0.086423772), \qquad (\varepsilon_2, \gamma_2) = (0.043172692, 0.949470320). \tag{6}$$

In Fig. 4, the red curves are the curves of "limit points" (or saddle-node bifurcation) of cycles. For parameter values (ε, γ) between the blue and red curves in Fig. 4, at least two limit cycles exist simultaneously, i.e., for γ close to 0 or γ close to 1, with a suitable $0 < \varepsilon \ll 1$, at least one stable and one unstable limit cycle coexist.

Remark 3. As we mentioned in Section 2.1, due to the property of "zero-order ultrasensitivity", the Michaelis-Menten constants and hence ε have to be small. Our observation from numerical simulations shows that, for sufficiently small ε, system (4) has similar qualitative behaviors when γ belongs to certain bounds which are close to 0 and 1. In this regard, we emphasize that although the position of the limit cycle changes when γ is close to 1 (see, for instance, Fig. 5), the geometric analysis of the dynamics is the same as the case that γ is close to 0, for sufficiently small ε.

Remark 4. In Section 2.1, we have unified all the Michaelis-Menten constants of system (1) by ε, resulted in system (4). Although γ has a similar size as the Michaelis-Menten constants, we have not unified it with them. The reason is that γ is the C-signal of the biological oscillator, i.e., the input under which the dynamics are triggered (see Fig. 1). Since such a signal coordinates the movements of the individual cells and influences the shape of the fruiting bodies [16], it is crucial to have γ in a certain range between 0 and 1. Our analysis throughout the paper clearly shows the role of γ.

2.3. Preliminaries on slow-fast systems

Our goal is to understand the dynamics of (4) for small ε in the limit $\varepsilon \to 0$. However, as it is seen in (4), when the variables f, c and e are very close to the boundary of $\mathcal{Q}$, the limiting behavior is different from the case that they are away from the boundary. To resolve the aforementioned problem, one possibility is to consider an auxiliary system which is smoothly equivalent to (4). To this end, let us define

$$H^{\varepsilon}(f, c, e) := H_1^{\varepsilon}(f) H_2^{\varepsilon}(c) H_3^{\varepsilon}(e),$$

where

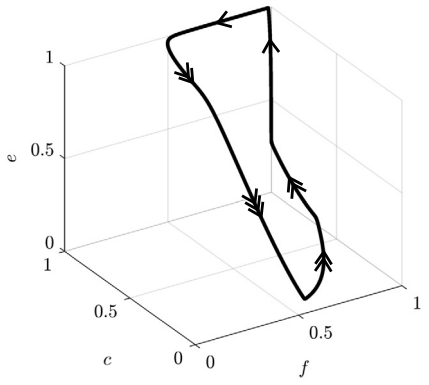

Fig. 5. Numerically computed attracting limit cycle of system (1) for $\varepsilon = 10^{-3}$ and $\gamma = 0.9$. The arrows indicate the direction and speed of the flow along the limit cycle. A single arrow corresponds to the slowest time scale, while three arrows indicate the fastest one.

$$\begin{aligned} H_1^\varepsilon(f) &:= (\varepsilon + 1 - f)(\varepsilon + 2f), \\ H_2^\varepsilon(c) &:= (\varepsilon + 2 - 2c)(\varepsilon + 2c), \\ H_3^\varepsilon(e) &:= (\varepsilon + 2 - 2e)(\varepsilon + 2e). \end{aligned} \tag{7}$$

Note that $H^\varepsilon(f, c, e) > 0$ for any $\varepsilon > 0$ and any $(f, c, e) \in \mathcal{Q}$. Therefore, we can reparametrize time of system (4) by multiplying both sides of (4) in $H^\varepsilon(f, c, e)$, which leads to the following dynamical system

$$\begin{aligned} \frac{df}{d\tau} &= \left(\frac{\gamma(1-f)}{\varepsilon + (1-f)} - \frac{2fe}{\varepsilon + 2f} \right) H^\varepsilon(f, c, e), \\ \frac{dc}{d\tau} &= \left(\frac{8(1-c)f}{\varepsilon + 2(1-c)} - \frac{4c}{\varepsilon + 2c} \right) H^\varepsilon(f, c, e), \\ \frac{de}{d\tau} &= \left(\frac{8(1-e)c}{\varepsilon + 2(1-e)} - \frac{4e}{\varepsilon + 2e} \right) H^\varepsilon(f, c, e), \end{aligned} \tag{8}$$

where, for simplicity, we recycle τ to denote the reparametrized time. One can rewrite (8) as follows

$$X_\varepsilon : \begin{cases} \frac{df}{d\tau} = [\gamma(1-f)(\varepsilon + 2f) - 2fe(\varepsilon + 1 - f)]\, H_2^\varepsilon(c) H_3^\varepsilon(e), \\ \frac{dc}{d\tau} = [8(1-c)f(\varepsilon + 2c) - 4c(\varepsilon + 2 - 2c)]\, H_1^\varepsilon(f) H_3^\varepsilon(e), \\ \frac{de}{d\tau} = [8(1-e)c(\varepsilon + 2e) - 4e(\varepsilon + 2 - 2e)]\, H_1^\varepsilon(f) H_2^\varepsilon(c). \end{cases} \tag{9}$$

The vector field (9) is smoothly equivalent to (4) for $\varepsilon > 0$ [1], which from now on is the object of study. The main reason to rewrite system (4) into the form of system (9) is that the latter is a singularly perturbed ODE which allows us to analyze the system using geometric methods. Moreover, note that in contrast to (4), system (9) is polynomial, which is another of its advantages.

2.3.1. Slow-fast systems

System (9) is a *slow-fast system in non-standard form*. Thus, in this section, we present a brief summary of the basic definitions and results regarding slow-fast systems of such a form. Our aim is to provide just necessary terminologies needed for this paper. For a detailed exposition, the reader is referred to [32].

A slow-fast system (SFS) *in standard form* is a singularly perturbed ordinary differential equation with two timescales often presented as

$$\begin{aligned} \dot{x} &= F(x, y, \varepsilon), \\ \varepsilon \dot{y} &= G(x, y, \varepsilon), \end{aligned} \tag{10}$$

where the dot $\dot{}$ denotes derivative with respect to the *slow* time t, F and G are assumed to be smooth, $x \in \mathbb{R}^{n_s}$, $y \in \mathbb{R}^{n_f}$, and $0 < \varepsilon \ll 1$ is a small parameter that describes the timescale separation between x and y. For details see [21].

In contrast, a slow-fast system *in non-standard form* is a vector field as

$$z' = Z(z, \varepsilon), \tag{11}$$

where $z \in \mathbb{R}^n$, $n \geq 2$, the prime $'$ denotes the derivative with respect to the fast time-parameter τ, and the smooth vector field $Z : \mathbb{R}^n \times \mathbb{R} \to \mathbb{R}^n$ is assumed to satisfy $Z(z, \varepsilon) = Z_0(z) + \varepsilon W(z, \varepsilon)$. One usually assumes that $\varepsilon \in (0, \varepsilon_0)$, with $\varepsilon \ll 1$. The main difference between (10) and (11) is that in system (11) there is no evident time scale separation between the components of z. As (11) is a perturbation problem, one usually starts its analysis by considering its unperturbed version.

Definition 1. The limit $\varepsilon \to 0$ of (11), that is

$$z' = Z(z, 0) = Z_0(z), \tag{12}$$

is called *the layer equation*.

The set of singularities of Z_0 has a crucial role in the analysis of (11), and allows one to distinguish whether (11) defines a regular or a singular perturbation problem:

Definition 2. Let

$$\mathcal{C} = \{x \in \mathbb{R}^n \mid Z(z, 0) = Z_0(z) = 0 \in \mathbb{R}^n\}. \tag{13}$$

Then:

- System (11) is a regular perturbation problem if the set $\mathcal{C}$ is either empty or it consists entirely of isolated singularities.
- System (11) is a singular perturbation problem if there exists a subset $\mathcal{C}_0 \subseteq \mathcal{C}$ which forms a k-dimensional, $1 \leq k < n$, differentiable manifold. The set $\mathcal{C}_0$ is called *the critical manifold* of (11).

Remark 5. In general, and as it happens in this paper, the set $\mathcal{C}_0$ is not necessarily a manifold. For example, it could be formed by the union, along lower dimensional submanifolds, of disjoint k-dimensional manifolds. Nevertheless, it is customary to keep referring to $\mathcal{C}_0$ as the critical manifold. One could refer to it as "the critical set" to avoid such ambiguity.

We note that generically, given that the critical manifold $\mathcal{C}_0$ is k-dimensional, the map $Z_0 : \mathbb{R}^n \to \mathbb{R}^n$ has constant rank $(n - k)$. This also implies that the Jacobian $\mathrm{D}Z_0$, evaluated at each point $z \in \mathcal{C}_0$, has at least k zero eigenvalues (called trivial eigenvalues) that correspond to the tangent space $T_z\mathcal{C}_0$, and $(n - k)$ *nontrivial* eigenvalues.

Definition 3. Let $\mathcal{C}_{0,n} \subseteq \mathcal{C}_0$ denote the subset where all nontrivial eigenvalues of $\mathrm{D}Z_0|_{\mathcal{C}_{0,n}}$ are nonzero, and let $\mathcal{C}_{0,h} \subseteq \mathcal{C}_{0,n}$ denote the subset where all nontrivial eigenvalues of $\mathrm{D}Z_0|_{\mathcal{C}_{0,h}}$ have nonzero real part. In the latter case, $\mathcal{C}_{0,h}$ is called *normally hyperbolic*. On the other hand, points in $\mathcal{C}_0 \backslash \mathcal{C}_{0,n}$ or in $\mathcal{C}_{0,n} \backslash \mathcal{C}_{0,h}$, if they exist, are called *non-hyperbolic*, and one says that "the critical manifold $\mathcal{C}_0$ loses normal hyperbolicity at such points".

If in (11) we rescale time by defining the slow time parameter $t = \varepsilon\tau$, one can rewrite (11) as

$$\dot{z} = \frac{1}{\varepsilon} Z_0(z) + W(z, \varepsilon). \tag{14}$$

The limit of (14) as $\varepsilon \to 0$, is called *the reduced problem* and is well defined if $z \in \mathcal{C}_0$ and the projection of $W(z, \varepsilon)$ to $\mathcal{C}_0$ is well defined (see [32, section 3.2]). The overall idea of Geometric Singular Perturbation Theory (GSPT) is to analyze the layer equation and the reduced problem, and then use perturbation arguments to describe the dynamics of (11).

One of the main results of Geometric Singular Perturbation Theory (GSPT) is concerned with slow-fast systems within a small neighborhood of a normally hyperbolic critical manifold.

Theorem 1 *(Fenichel [7]). Let $\mathcal{S}_0 \subseteq \mathcal{C}_{0,h}$ be a* compact *and normally hyperbolic critical manifold of a SFS* (11)*. Then, for $\varepsilon > 0$ sufficiently small, the following holds:*

- *There exists a locally invariant manifold $\mathcal{S}_\varepsilon$ which is diffeomorphic to $\mathcal{S}_0$ and lies within distance of order $O(\varepsilon)$ from $\mathcal{S}_0$.*
- *The flow on $\mathcal{S}_\varepsilon$ converges to the reduced flow on $\mathcal{S}_0$ as $\varepsilon \to 0$.*
- *$\mathcal{S}_\varepsilon$ has the same stability properties as $\mathcal{S}_0$.*

In a nutshell, Fenichel's theorem implies that the dynamics of the slow-fast system (11) near a compact and normally hyperbolic critical manifold is a regular perturbation of the reduced problem. On the other hand, the dynamics near non-hyperbolic points can be quite intricate. In the next section we briefly present a powerful technique to study the dynamics of slow-fast systems near a class of non-hyperbolic points.

2.3.2. The blow-up method

The blow-up method was introduced to describe the dynamics of SFSs near non-hyperbolic points, and is the main mathematical technique used in forthcoming section of this article. Here we just provide a brief description of the method, for more details the interested reader is referred to [6,17,20,21].

Definition 4. Consider a generalized polar coordinate transformation

$$\begin{aligned} &\Phi : \mathbb{S}^n \times I \to \mathbb{R}^{n+1} \\ &\Phi(\bar{z}, \bar{\varepsilon}, \bar{r}) \mapsto (\bar{r}^\alpha \bar{z}, \bar{r}^\gamma \bar{\varepsilon}) = (z, \varepsilon), \end{aligned} \tag{15}$$

where $\sum_{i=1}^n \bar{z}_i^2 + \bar{\varepsilon}^2 = 1$ and $\bar{r} \in I$ where I is a (possibly infinite) interval containing $0 \in \mathbb{R}$. The corresponding *(quasi-homogeneous)*[5] *blow-up* is defined by $(\bar{z}, \bar{\varepsilon}, \bar{r}) = \Phi^{-1}(z, \varepsilon)$. The map Φ is called *blow down*.[6]

For the purposes of this article, it is sufficient to let $\bar{r} \in [0, \rho)$, with $\rho > 0$. The main idea of the blow-up method is to construct a new, but equivalent, vector field to Z (11), which is defined in a higher dimensional manifold, but whose singularities are simpler compared to those of Z.

Definition 5. The blown up vector field $\bar{Z}$ is induced by the blow-up map as $\bar{Z} = \mathrm{D}\Phi^{-1} \circ Z \circ \Phi$, where $\mathrm{D}\Phi$ denotes the derivative of Φ. If $\bar{Z}$ vanishes on $\mathbb{S}^n \times \{0\}$ with order $m \in \mathbb{N}$, we define *the desingularized vector field* $\tilde{Z} = \frac{1}{\bar{r}^m} \bar{Z}$.

[5] A homogeneous blow-up (or simply blow-up) refers to all the exponents α, β, γ set to 1.
[6] Note that the blow-up maps the origin $0 \in \mathbb{R}^{n+1}$ to the sphere $\mathbb{S}^n \times \{0\}$ while the blow down does the opposite, hence the names.

Note that the vector fields Z and $\tilde{Z}$ are equivalent on $\mathbb{S}^n \times \{\bar{r} > 0\}$. Moreover, if the weights (α, γ) are well chosen, the singularities of $\tilde{Z}|_{\bar{r}=0}$ are partially hyperbolic or even hyperbolic, making the analysis of $\tilde{Z}$ simpler than that of Z. Due to the equivalence between Z and $\tilde{Z}$, one obtains all the local information of Z around $0 \in \mathbb{R}^{n+1}$ from the analysis of $\tilde{Z}$ around $\mathbb{S}^n \times \{\bar{r} \geq 0\}$.

While doing computations, it is more convenient to study the vector field $\tilde{Z}$ in charts. A chart is a parametrization of a hemisphere of $\mathbb{S}^n \times I$ and is obtained by setting one of the coordinates $(\bar{z}, \bar{\varepsilon}) \in \mathbb{S}^n$ to ± 1 in the definition of Φ. For example, one of the most important charts in the blow-up method is the central chart defined by $K_{\bar{\varepsilon}} = \{\bar{\varepsilon} = 1\}$. After we study the dynamics in the relevant charts, we connect the flow together via *transition maps*, allowing us a complete description of the flow of $\tilde{Z}$ near $\mathbb{S}^n \times \{0\}$. In turn, and as mentioned above, the flow of $\tilde{Z}$ is equivalent to the flow of Z for $\varepsilon > 0$ sufficiently small. For more details see Section 4 and [17,21].

Remark 6. It is also possible to blow-up *only some* of the variables in the system (11), and keep the others unchanged. In this paper, we blow-up a non-hyperbolic line of equilibria to a cylinder, see Section 4.

3. Geometric singular perturbation analysis

The goal of this section is to give the detailed analysis of the slow-fast structure of the auxiliary system (9).

3.1. Layer problem and the critical manifold

Setting $\varepsilon = 0$ in (9) results in the layer problem

$$\begin{aligned} \frac{df}{d\tau} &= (\gamma - e)\, H^0(f, c, e), \\ \frac{dc}{d\tau} &= 2\,(2f - 1)\, H^0(f, c, e), \\ \frac{de}{d\tau} &= 2(2c - 1) H^0(f, c, e), \end{aligned} \tag{16}$$

with

$$H^0(f, c, e) = 32 f c e (1 - f)(1 - c)(1 - e).$$

Apart form the isolated equilibrium point $P := (0.5, 0.5, \gamma)$, which is inside the cube $\mathcal{Q}$, the boundary of $\mathcal{Q}$, which consists of six planes, is the equilibria set of the layer problem (16). We denote each plane of equilibria by $\mathcal{S}_{0,i}$ $(i = 1, 2, ..., 6)$ as follows:

$$\begin{aligned} \mathcal{S}_{0,1} &:= \left\{(f, c, e) \in \mathbb{R}^3 \,|\, f = 0,\ c \in [0, 1],\ e \in [0, 1]\right\}, \\ \mathcal{S}_{0,2} &:= \left\{(f, c, e) \in \mathbb{R}^3 \,|\, f \in [0, 1],\ c = 0,\ e \in [0, 1]\right\}, \\ \mathcal{S}_{0,3} &:= \left\{(f, c, e) \in \mathbb{R}^3 \,|\, f \in [0, 1],\ c \in [0, 1],\ e = 0\right\}, \\ \mathcal{S}_{0,4} &:= \left\{(f, c, e) \in \mathbb{R}^3 \,|\, f = 1,\ c \in [0, 1],\ e \in [0, 1]\right\}, \\ \mathcal{S}_{0,5} &:= \left\{(f, c, e) \in \mathbb{R}^3 \,|\, f \in [0, 1],\ c = 1,\ e \in [0, 1]\right\}, \\ \mathcal{S}_{0,6} &:= \left\{(f, c, e) \in \mathbb{R}^3 \,|\, f \in [0, 1],\ c \in [0, 1],\ e = 1\right\}. \end{aligned} \tag{17}$$

Therefore $\mathcal{S}_0 := \bigcup_{i=1}^{6} \mathcal{S}_{0,i}$ is the critical manifold. The stability of system (9) changes at lines $\ell_f \in \mathcal{S}_{0,2}$, $\ell^f \in \mathcal{S}_{0,5}$ (given by $f = f^*$); $\ell_c \in \mathcal{S}_{0,3}$, $\ell^c \in \mathcal{S}_{0,6}$ (given by $c = c^*$); and $\ell_e \in \mathcal{S}_{0,1}$, $\ell^e \in \mathcal{S}_{0,4}$ (given by $e = e^*$).

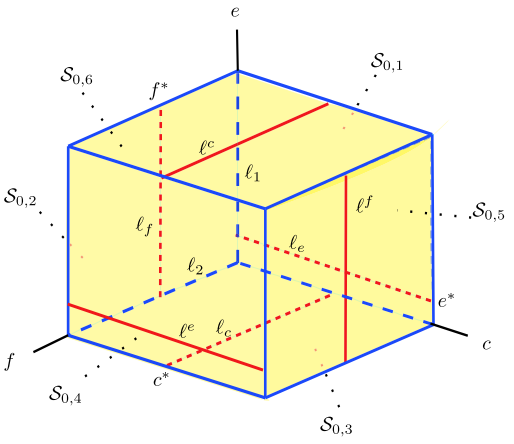

Fig. 6. The critical manifold $\mathcal{S}_0 = \bigcup_{i=1}^{6} \mathcal{S}_{0,i}$, non-hyperbolic lines $\ell_f, \ell_c, \ell_e, \ell^f, \ell^c, \ell^e$ in red, all 12 non-hyperbolic edges in blue, and in particular, the two non-hyperbolic edges ℓ_1 and ℓ_2 shall play an important role in our analysis.

Moreover, the 12 edges of the unit cube, where the 6 planes $\mathcal{S}_{0,i}$ intersect, are non-hyperbolic lines as well. However, for our analysis, only the lines $\ell_1 = \mathcal{S}_{0,1} \cap \mathcal{S}_{0,2}$ and $\ell_2 = \mathcal{S}_{0,2} \cap \mathcal{S}_{0,3}$ are crucial (see Fig. 6). The stability of points in $\mathcal{S}_0$ is summarized in the following lemma.

Lemma 1. *The critical manifold $\mathcal{S}_0$ of the layer problem (16) has the following properties:*

- *$\mathcal{S}_{0,1}$ is attracting for $e > e^*$ and repelling for $e < e^*$.*
- *$\mathcal{S}_{0,2}$ is attracting for $f < f^*$ and repelling for $f > f^*$.*
- *$\mathcal{S}_{0,3}$ is attracting for $c < c^*$ and repelling for $c > c^*$.*
- *$\mathcal{S}_{0,4}$ is attracting for $e < e^*$ and repelling for $e > e^*$.*
- *$\mathcal{S}_{0,5}$ is attracting for $f > f^*$ and repelling for $f < f^*$.*
- *$\mathcal{S}_{0,6}$ is attracting for $c > c^*$ and repelling for $c < c^*$.*
- *The equilibrium $P := (0.5, 0.5, \gamma)$ is a saddle-focus point.*
- *The lines $\ell_f \in \mathcal{S}_{0,1}, \ell_c \in \mathcal{S}_{0,2}, \ell_e \in \mathcal{S}_{0,3}, \ell^f \in \mathcal{S}_{0,4}, \ell^c \in \mathcal{S}_{0,5}, \ell^e \in \mathcal{S}_{0,6}$, all 12 edges of the unit cube, and in particular, the edges $\ell_1 = \mathcal{S}_{0,1} \cap \mathcal{S}_{0,2}$ and $\ell_2 = \mathcal{S}_{0,2} \cap \mathcal{S}_{0,3}$ are non-hyperbolic.*

Proof. The eigenvalues of the linearization of system (16) at points, e.g., in the plane $\mathcal{S}_{0,1}$ are given by

$$\lambda_1 = \lambda_2 = 0, \qquad \lambda_3 = -32ce(c-1)(e-1)(e-\gamma).$$

It is clear that λ_3 is zero at the boundary of $\mathcal{S}_{0,1}$, and also along the line l_e given by $e = e^*$. Therefore, $\mathcal{S}_{0,1}$ is attracting for $e > e^*$ and it is repelling for $e < e^*$. The proof of the other cases is performed analogously. □

We denote the interior of the cube $\mathcal{Q}$ by $\mathring{\mathcal{Q}}$. Note that when $(f, c, e) \in \mathring{\mathcal{Q}}$, the layer problem (16) can be divided by the positive term $H^0(f, c, e) = 32fce(1-f)(1-c)(1-e)$. Therefore away from the critical manifold S, all the variables evolve on the fast time scale τ and the orbits of the layer problem (16) are identical to the orbits of the linear system

$$\begin{aligned} \frac{df}{d\tau} &= \gamma - e, \\ \frac{dc}{d\tau} &= 2(2f-1), \\ \frac{de}{d\tau} &= 2(2c-1). \end{aligned} \tag{18}$$

Table 1
For each row i we show the interval of definition of $\mathcal{S}^{\mathrm{a}}_{\varepsilon,i}$ and the relation by which it is defined, all analogous to Lemma 2.

i	I^{a}_i	$\mathcal{S}^{\mathrm{a}}_{\varepsilon,i}$
2	$(f,e)\in[\delta,\ \frac{1}{2}-\delta]\times[\delta,\ 1-\delta]$	$c=\frac{f}{1-2f}\varepsilon+O(\varepsilon^2)$
3	$(f,c)\in[\delta,\ 1-\delta]\times[\delta,\ \frac{1}{2}-\delta]$	$e=\frac{c}{1-2c}\varepsilon+O(\varepsilon^2)$
6	$(f,c)\in[\delta,\ 1-\delta]\times[\frac{1}{2}+\delta,1-\delta]$	$e=1+\frac{1}{2(1-2c)}\varepsilon+O(\varepsilon^2)$

Remark 7. System (18) is the limit of (4) when $\varepsilon\to 0$ and $(f,c,e)\in\mathring{\mathcal{Q}}$.

3.2. Reduced problem, slow manifolds, and slow dynamics

From Subsection 3.1, we know that the boundary of $\mathcal{Q}$ is the critical manifold $\mathcal{S}_0$. Any compact subset of $\mathcal{S}_0$ that does not contain any non-hyperbolic point is normally hyperbolic, and hence Fenichel theory [7] is applicable. In other words, this theory implies that the normally hyperbolic parts of $\mathcal{S}_0$ perturb to slow manifolds, which lie within a distance of order $O(\varepsilon)$ of the critical manifold $\mathcal{S}_0$. In the following, we compute the slow manifolds and analyze the reduced flows in the planes $\mathcal{S}_{0,1}$, $\mathcal{S}_{0,2}$, $\mathcal{S}_{0,3}$ and $\mathcal{S}_{0,6}$ which are essential for our analysis.

Lemma 2. *For sufficiently small $\delta>0$, there exist $\varepsilon_0>0$ and a smooth function $h_{\varepsilon,1}(c,e)$ defined on $I^a_1=[\delta,\ 1-\delta]\times[\gamma+\delta,\ 1-\delta]$ such that the manifold*

$$\mathcal{S}^a_{\varepsilon,1}=\{(f,c,e)\in\mathcal{Q}\,|\,f=h_{\varepsilon,1}(c,e),\ (c,e)\in I^a_1\}\,, \tag{19}$$

is a locally invariant attracting manifold of (9) for $\varepsilon\in(0,\varepsilon_0]$. The function $h_{\varepsilon,1}(c,e)$ has the expansion

$$h_{\varepsilon,1}(c,e)=\frac{\gamma}{2(e-\gamma)}\varepsilon+O(\varepsilon^2). \tag{20}$$

Proof. Since the set I^{a}_1 is hyperbolic, Fenichel theory implies that there exists a sufficiently small $\varepsilon_0>0$ such that the function $h_{\varepsilon,1}(c,e)$ has the expansion $h_{\varepsilon,1}(c,e)=\eta(c,e)\varepsilon+O(\varepsilon^2)$ for all $\varepsilon\in(0,\varepsilon_0]$. Due to invariance, we can substitute $h_{\varepsilon,1}(c,e)$ into the equation of $\frac{df}{d\tau}$ in (9) and identify coefficients of ε. By doing so, we obtain

$$\eta(c,e)=\frac{\gamma}{2(e-\gamma)}. \tag{21}$$

Note that (21) reflects the fact that the manifold $\mathcal{S}^{\mathrm{a}}_{\varepsilon,1}$ is not well-defined when $e=\gamma$. Thus, the invariant manifold $\mathcal{S}^{\mathrm{a}}_{\varepsilon,1}$ is given as stated in the lemma, which completes the proof. □

For the sake of brevity, we summarize the analysis in the planes $\mathcal{S}_{0,2}$, $\mathcal{S}_{0,3}$ and $\mathcal{S}_{0,6}$ in Table 1, which is shown by following the same line of reasoning as the one of Lemma 2. For more details, the interested reader is referred to [27].

Remark 8. Similar results can be obtained for the "repelling" parts $\mathcal{S}^{\mathrm{r}}_{\varepsilon,i}$, $i=1,2,...,6$. However, these are not needed in our analysis. Nonetheless, we point out that the slow manifolds $\mathcal{S}^{\mathrm{r}}_{\varepsilon,i}$ would be expressed by the same functions $h_{\varepsilon,i}$ and appropriate intervals I^{r}_i.

Remark 9. The expansions of the functions $h_{\varepsilon,i}(\cdot,\cdot)$, $i=1,2,3,6$, also explain why it is necessary to restrict the domain of definition of the slow manifolds to I^{a}_i to exclude their singularities.

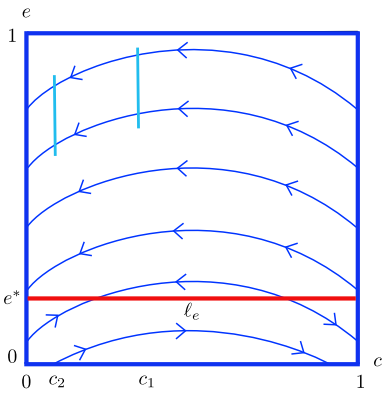

Fig. 7. Flow of the slow vector field in $\mathcal{S}_{0,1}$, non-hyperbolic line ℓ_e in red, and sections c_1, c_2 in cyan.

We now turn to the analysis of the reduced flows in the planes $\mathcal{S}_{0,1}$, $\mathcal{S}_{0,2}$, $\mathcal{S}_{0,3}$ and $\mathcal{S}_{0,6}$ which, respectively, means the planes $f = 0, c = 0, e = 0$ and $e = 1$. We know that system (9) has the fast time scale τ. By substituting the functions $h_{\varepsilon,i}$, $i = 1, 2, 3, 6$ into (9), transforming the fast time variable to the slow one by $t = \varepsilon\tau$, and setting $\varepsilon = 0$, the equations governing the slow dynamics on the critical manifold $\mathcal{S}_{0,i}$ are computed. In the following, we give the analysis in the plane $\mathcal{S}_{0,1}$.

After substituting $h_{\varepsilon,1}$ into system (9), the dynamics of the reduced system in $\mathcal{S}_{0,1}$, i.e., on the plane $f = 0$, is governed by

$$\begin{aligned} c' &= \frac{-32ce^2(c-1)(e-1)}{e-\gamma}\varepsilon + O(\varepsilon^2), \\ e' &= \frac{32ce^2(c-1)(e-1)(2c-1)}{e-\gamma}\varepsilon + O(\varepsilon^2), \end{aligned} \tag{22}$$

where $'$ denotes the differentiation with respect to τ. Now by dividing out a factor of ε, which corresponds to switching from the fast time variable to the slow one, we have

$$\begin{aligned} \dot{c} &= \frac{-32ce^2(c-1)(e-1)}{e-\gamma} + O(\varepsilon), \\ \dot{e} &= \frac{32ce^2(c-1)(e-1)(2c-1)}{e-\gamma} + O(\varepsilon), \end{aligned} \tag{23}$$

where the overdot represents differentiation with respect to $t = \varepsilon\tau$. Now, by setting $\varepsilon = 0$ in (23), the reduced flow on $\mathcal{S}_{0,1}$ is given by

$$\begin{aligned} \dot{c} &= \frac{-32ce^2(c-1)(e-1)}{e-\gamma}, \\ \dot{e} &= \frac{32ce^2(c-1)(e-1)(2c-1)}{e-\gamma}. \end{aligned} \tag{24}$$

As it is clear, the vector field (24) is singular at the line ℓ_e, given by $e = e^*$. In other words, the flow (24) is not defined on the line ℓ_e. The lines $c = 0$, $e = 0$, $c = 1$, and $e = 1$, shown in Fig. 7, are lines of equilibria. The line $c = 0$ is attracting for $e > e^*$ and it is repelling for $e < e^*$, while the line $c = 1$ is attracting for $e < e^*$ and repelling for $e > e^*$.

By dividing out the factor $\frac{32ce^2(c-1)(e-1)}{e-\gamma}$ in (24), the orbits of the reduced flow can be derived from the desingularized system

$$\begin{aligned} \dot{c} &= -1, \\ \dot{e} &= 2c - 1, \end{aligned} \tag{25}$$

which can be integrated explicitly.

Remark 10. For $e > e^*$, systems (24) and (25) have qualitatively the same dynamics when $c, e \in (0, 1)$. In particular, the vector field (25) is C^∞-equivalent but not C^∞-conjugate to the vector field (24). For the case that $e < e^*$, the direction of the vector field (24) is not preserved in the vector field (25). However, for our analysis, it suffices to study the flow of system (24) when $e > e^*$, or equivalently on $\mathcal{S}^{\mathrm{a}}_{0,1}$.

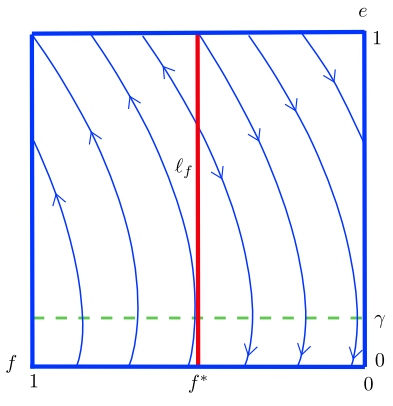

(a) The desingularized slow flow along $\mathcal{S}_{0,2}$ is

$$\begin{aligned} \dot{f} &= \gamma - e \\ \dot{e} &= -2. \end{aligned} \tag{26}$$

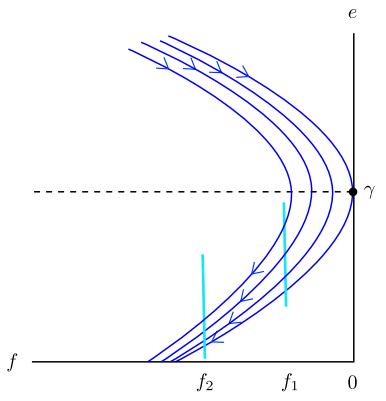

(b) The slow flow of vector field (26) along $\mathcal{S}_{0,2}$ around $e = \gamma$ as well as the sections f_1, f_2 in cyan close to zero. Note that the variable f is tangent to the line $f = 0$ at $e = \gamma$.

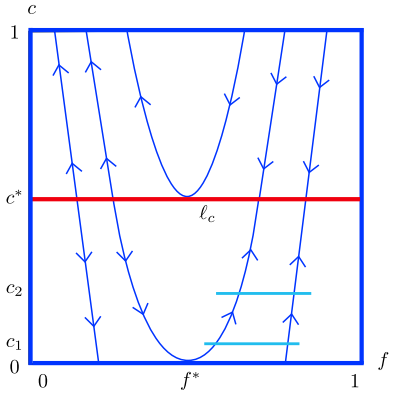

(c) The desingularized slow flow along $\mathcal{S}_{0,3}$ is

$$\begin{aligned} \dot{f} &= \gamma, \\ \dot{c} &= 2(2f - 1). \end{aligned} \tag{27}$$

For $f > f^*$, the reduced flow (27) contracts the variable f between sections $c = c_1$ and $c = c_2$ with $0 < c_1 < c < c_2 < c^*$.

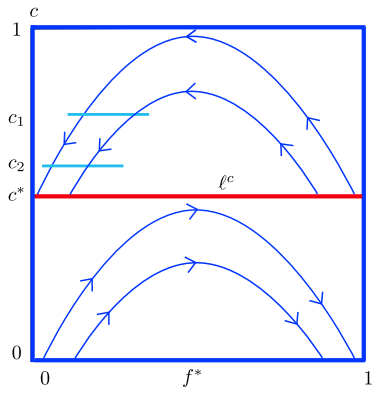

(d) The desingularized slow flow along $\mathcal{S}_{0,6}$ is

$$\begin{aligned} \dot{f} &= \gamma - 1, \\ \dot{c} &= 2f - 1. \end{aligned} \tag{28}$$

For $f < f^*$, the reduced flow (28) contracts the variable f between sections $c = c_1$ and $c = c_2$ with $c^* < c_1 < c < c_2 < 1$.

Fig. 8. The reduced flows along $\mathcal{S}^{\mathrm{a}}_{0,2}$, $\mathcal{S}^{\mathrm{a}}_{0,3}$ and $\mathcal{S}^{\mathrm{a}}_{0,6}$. The vector fields are singular at red lines. The thick blue lines are lines of equilibria. The direction of vector fields shows which (part of) line of equilibria is either attracting or repelling.

Lemma 3. *For $e > e^*$, the reduced flow (24) on $\mathcal{S}_{0,1}$ and hence the slow flow (23) on $\mathcal{S}^a_{\varepsilon,1}$ maps section $\{c = c_1\}$ to $\{c = c_2\}$, where $0 < c_2 < c_1 < \frac{1}{2}$; this map is well-defined and its first derivative with respect to e is equal to one.*

Proof. It suffices to consider (25). Let $\Pi(e)$ denote the map from $\{c = c_1\}$ to $\{c = c_2\}$ induced by the flow of (25). Then, it is straightforward to get $\Pi(e) = e + c_2 - c_2^2 - c_1 + c_1^2$, from which the statement follows. □

In order to obtain the equations governing the slow flow along $\mathcal{S}^{\mathrm{a}}_{\varepsilon,2}$, $\mathcal{S}^{\mathrm{a}}_{\varepsilon,3}$ and $\mathcal{S}^{\mathrm{a}}_{\varepsilon,6}$, a similar analysis can be done by inserting the functions $h_{\varepsilon,2}$, $h_{\varepsilon,3}$ and $h_{\varepsilon,6}$ into (9) and dividing out a factor of ε, which corresponds to switching to the slow time scale $t = \varepsilon\tau$. Next, by setting $\varepsilon = 0$ one obtains the reduced flow on the critical manifolds $\mathcal{S}_{0,2}$, $\mathcal{S}_{0,3}$ and $\mathcal{S}_{0,6}$. For the sake of brevity, we have summarized the slow flows along $\mathcal{S}_{0,2}$, $\mathcal{S}_{0,3}$ and $\mathcal{S}_{0,6}$ in Fig. 8. For more details, the interested reader is referred to [27].

3.3. Singular cycle

In this section, we present the overall behavior of the singular cycle, which is a closed curve consisting of alternating parts of the layer problem, and the critical manifold $\mathcal{S}_0$. However, by the information that we have so far from the critical manifold and the layer problem, we cannot fully describe the singular cycle close to the non-hyperbolic lines ℓ_1 and ℓ_2. A full description of the singular cycle for those parts that cannot be derived from the critical manifold and the layer problem is presented in Section 4 by the blow-up method.

The construction of the singular cycle Γ_0 starts at the point $p^f := (0.5, 0, 0)$. This point is connected to the point $p_1 := (\frac{1+\sqrt{\gamma}}{2}, 0.5, 0) \in \ell_c$ through the orbit ω_1 of the reduced flow (27). Starting at p_1, the layer problem (18) intersects the attracting part of the plane $\mathcal{S}^{\mathrm{a}}_{0,6}$ in a point, denoted by p_2. This point is connected to a point, denoted by $q^e \in \ell^c$, through the orbit ω_3 of the reduced flow (28). Starting at q^e, through the layer problem (18), the orbit ω_4 intersects the plane $\mathcal{S}^{\mathrm{a}}_{0,1}$ at a point, denoted by q_e. The orbit ω_5 of the reduced flow (22) connects q_e to a point, denoted by $p^e \in \ell_1$, which is the intersection of $\mathcal{S}^{\mathrm{a}}_{0,1}$ and $\mathcal{S}^{\mathrm{a}}_{0,2}$; p^e is connected to the point $p_e := (0, 0, \gamma)$ by a segment on the line ℓ_1, denoted by ω_6. The orbit ω_7 of the reduced flow (26) connects p_e to the point $p_f := (\frac{\gamma^2}{4}, 0, 0)$; Finally, p_f is connected to p^f by a segment on the line ℓ_2, denoted by ω_8. Hence, the singular cycle $\Gamma_0 \in \mathbb{R}^3$ of system (9) for $\varepsilon = 0$ is defined as follows (see Fig. 9):

$$\Gamma_0 := \omega_1 \cup \omega_2 \cup \omega_3 \cup \omega_4 \cup \omega_5 \cup \omega_6 \cup \omega_7 \cup \omega_8. \tag{29}$$

Remark 11. All the orbits ω_j $(j = 1, 2, ..., 8)$ are known analytically.

Owing to the fact that the layer problem is linear, all the points that connect ω_j to ω_{j+1} are explicitly known. For the particular quantity $\gamma = 0.08$, we have $p^f = (0.5, 0, 0)$, $p_1 \approx (0.6414, 0.5, 0)$, $p_2 \approx (0.3638, 0.8485, 1)$, $q^e \approx (0.0771, 0.5, 1)$, $q_e \approx (0, 0.3438, 0.9743)$, $p^e \approx (0, 0, 0.7487)$, $p_e = (0, 0, 0.08)$, and $p_f = (0.0016, 0, 0)$.

Remark 12. At the singular level, there is no visible flow on the segments ω_6 and ω_8. The blow-up analysis, carried out in Section 4, will reveal a hidden flow for such segments.

3.4. Main result

In view of the singular cycle Γ_0, introduced in the previous subsection, we are now ready to present the main result.

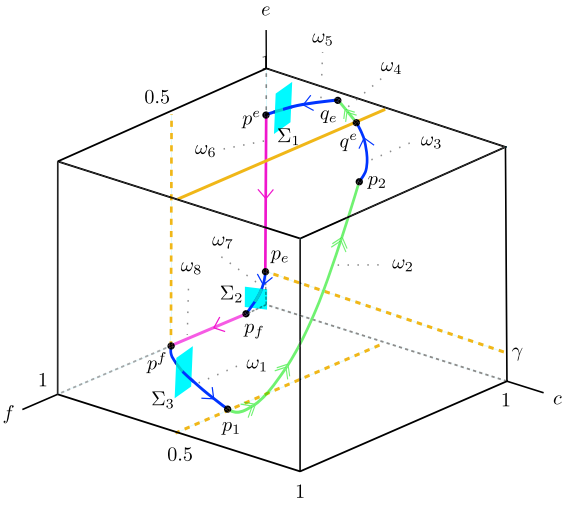

Fig. 9. Schematic diagram of the singular cycle Γ_0.

Theorem 2. *Assume that Γ_0 is the singular cycle described in Section 3.3. Then for sufficiently small $\varepsilon > 0$, there exists a unique attracting periodic orbit Γ_ε of the auxiliary system (9), which tends to the singular cycle Γ_0 as $\varepsilon \to 0$.*

In order to prove Theorem 2, we need to introduce the following sections

$$\begin{aligned}
\Sigma_1 &:= \{(f,c,e) \in \mathbb{R}^3 \mid (f,\ e) \in R_1,\ c = \delta_1\},\\
\Sigma_2 &:= \{(f,c,e) \in \mathbb{R}^3 \mid (c,\ e) \in R_2,\ f = \delta_2\},\\
\Sigma_3 &:= \{(f,c,e) \in \mathbb{R}^3 \mid (f,\ e) \in R_3,\ c = \delta_3\},
\end{aligned} \tag{30}$$

where R_j $(j = 1,2,3)$ are suitable small rectangles, and δ_j are chosen sufficiently small. Note that Σ_1 is transversal to ω_4, Σ_2 is transversal to ω_6, and Σ_3 is transversal to ω_8, see Fig. 9.

According to the definition of the sections Σ_i, introduced in (30), we define the following Poincaré maps for the flow of the system (9)

$$\begin{aligned}
&\pi_1 : \Sigma_1 \to \Sigma_2,\\
&\pi_2 : \Sigma_2 \to \Sigma_3,\\
&\pi_3 : \Sigma_3 \to \Sigma_1,
\end{aligned} \tag{31}$$

where the map π_1 describes the passage from Σ_1 to Σ_2 along the non-hyperbolic line ℓ_1, the map π_2 describes the passage from Σ_2 to Σ_3 along the non-hyperbolic line ℓ_2, and the map π_3 describes the passage from Σ_3 to Σ_1. The map π_3 consists of slow flow along $\mathcal{S}^{\mathrm{a}}_{\varepsilon,3}$, followed by the fast dynamics from a neighborhood of p_1 to a neighborhood of p_2, followed by the slow flow along $\mathcal{S}^{\mathrm{a}}_{\varepsilon,6}$ to a neighborhood of q^e. Through the fast dynamics, this neighborhood is mapped to a neighborhood of q_e, followed by the slow flow along $\mathcal{S}^{\mathrm{a}}_{\varepsilon,1}$ to Σ_1.

We summarize the properties of the above maps in the following lemmas.

Lemma 4. *If the section Σ_1 is chosen sufficiently small, then there exists $\varepsilon_0 > 0$ such that the map*

$$\pi_1 : \Sigma_1 \to \Sigma_2, \qquad (f,e) \mapsto (\pi_1^c(f,e,\varepsilon), \pi_1^e(f,e,\varepsilon)), \tag{32}$$

is well-defined for $\varepsilon \in [0, \varepsilon_0]$ *and smooth for* $\varepsilon \in (0, \varepsilon_0]$. *The map* π_1 *is a strong contraction with contraction rate* $\exp(-K/\varepsilon)$ *for some* $K > 0$. *The image of* Σ_1 *is a two-dimensional domain of exponentially small size, which converges to the point* $q_2 := \Sigma_2 \cap \omega_7$ *as* $\varepsilon \to 0$.

Lemma 5. *If the section* Σ_2 *is chosen sufficiently small, then there exists* $\varepsilon_0 > 0$ *such that the map*

$$\pi_2 : \Sigma_2 \to \Sigma_3, \qquad (c, e) \mapsto (\pi_2^f(c, e, \varepsilon), \pi_2^e(c, e, \varepsilon)), \tag{33}$$

is well-defined for $\varepsilon \in [0, \varepsilon_0]$ *and smooth for* $\varepsilon \in (0, \varepsilon_0]$. *The map* π_2 *is a strong contraction with contraction rate* $\exp(-K/\varepsilon)$ *for some* $K > 0$. *The image of* Σ_2 *is a two-dimensional domain of exponentially small size, which converges to the point* $q_3 := \Sigma_3 \cap \omega_1$ *as* $\varepsilon \to 0$.

The proofs of Lemmas 4 and 5 are based on the blow-up analysis of the lines ℓ_1 and ℓ_2, respectively, which will be presented in Subsections 4.1 and 4.2.

Remark 13. The points on the line ℓ_c when $0.5 < f < 1$, and on the line ℓ^c when $0 < f < 0.5$ are jump fold points, i.e., the trajectory switches from the slow dynamics to the fast dynamics. One way of showing the aforementioned is by following [24, Lemma 6]. For the reader's convenience, we have included such computations in Appendix B. This also explains why the behavior of the trajectory near ℓ_c is very similar to the behavior of standard slow-fast systems with two slow variables and one fast variable near a generic "fold" line, studied in [26] based on the blow-up method. The critical manifolds $\mathcal{S}_{0,3}$ and $\mathcal{S}_{0,6}$ of system (9) can be viewed as a standard folded critical manifold, which has been straightened out by a suitable diffeomorphism. This leads to the curved fibers of the layer problem (16). Therefore, we can use the results of [26] to understand the behavior of (9) close to the non-hyperbolic lines ℓ_c and ℓ^c.

The following lemma describes the map from the section Σ_3 to the section Σ_1, defined in (31).

Lemma 6. *If the section* Σ_3 *is chosen sufficiently small, then there exists* $\varepsilon_0 > 0$ *such that the map*

$$\pi_3 : \Sigma_3 \to \Sigma_1, \qquad (f, e) \mapsto (\pi_3^f(f, e, \varepsilon), \pi_3^e(f, e, \varepsilon)), \tag{34}$$

is well-defined for $\varepsilon \in [0, \varepsilon_0]$ *and smooth for* $\varepsilon \in (0, \varepsilon_0]$. *The image of* Σ_3 *is an exponentially thin strip lying exponentially close to* $S^1_{a,\varepsilon} \cap \Sigma_1$, *i.e., its width in the* f*-direction is* $O(\exp(-K/\varepsilon))$ *for some* $K > 0$. *Moreover,* $\pi_3(\Sigma_3)$ *converges to a segment of* $\mathcal{S}^a_{0,1} \cap \Sigma_1$ *as* $\varepsilon \to 0$.

Proof. The basic idea of the proof is based on the map that has been already described in Fig. 9 for $\varepsilon = 0$, denoted by π_3^0, and then treat π_3 as an ε-perturbation of π_3^0. If the section Σ_3 is chosen sufficiently small, then the trajectories starting in Σ_3 can be described by the slow flow along the manifold $\mathcal{S}^{\mathrm{a}}_{\varepsilon,3}$ combined with the exponential contraction towards the slow manifold until they reach a neighborhood of the jump points on the line ℓ_c. Applying [26, Theorem 1] close to the jump pints, the trajectories switch from the slow dynamics to the fast dynamics, and hence pass the non-hyperbolic line ℓ_c; this transition is well-defined for $\varepsilon \in [0, \varepsilon_1]$, and smooth for $\varepsilon \in (0, \varepsilon_1]$ for some $\varepsilon_1 > 0$. Note that [26, Theorem 1] guarantees that the contraction of the solutions in the e-direction persists during the passage through the fold-line ℓ_c, as it is at most algebraically expanding. After that, the solutions follow the fast dynamics ω_2 until they reach a neighborhood of the point p_2, see Fig. 9. Next, the solutions follow the slow flow along the manifold $\mathcal{S}^{\mathrm{a}}_{\varepsilon,6}$ combined with the exponential contraction towards the slow manifold until they reach a neighborhood of the point q^e. Again applying [26, Theorem 1] close to the jump points, the solutions which are very close to the non-hyperbolic line ℓ^c switch from the slow dynamics to the fast dynamics, and hence pass the non-hyperbolic line ℓ^c, where the corresponding transitions are well-defined for $\varepsilon \in [0, \varepsilon_2]$, and smooth for

$\varepsilon \in (0, \varepsilon_2]$ for some $\varepsilon_2 > 0$, and then follow the fast dynamics (ω_4) until they reach a neighborhood of the point q_e. Finally, the solutions follow the slow flow along the manifold $\mathcal{S}^{\mathrm{a}}_{\varepsilon,1}$ combined with the exponential contraction towards the slow manifold until they reach the section Σ_1.

Theorem 1 of [26] implies that the map π_3 is at most algebraically expanding in the direction of e when Σ_3 is chosen sufficiently small. On the other hand, the slow manifold $\mathcal{S}^{\mathrm{a}}_{\varepsilon,1}$ is exponentially contracting in the direction of f (Fenichel theory). Therefore, the image of Σ_3 is a thin strip lying exponentially close to $\mathcal{S}^{\mathrm{a}}_{\varepsilon,1} \cap \Sigma_1$. Hence, the statements of the lemma follow. □

Now we are ready to give the proof of the main result.

Proof of Theorem 2. Let us define the map $\pi : \Sigma_3 \to \Sigma_3$ as a combination of the maps π_j $(j = 1, 2, 3)$, described in Lemmas 4, 5 and 6. More precisely, we define

$$\pi = \pi_2 \circ \pi_1 \circ \pi_3 : \Sigma_3 \to \Sigma_3.$$

If the section Σ_3 is chosen sufficiently small, Lemma 6 implies that there exists $\varepsilon_3 > 0$ such that the map π_3 is well-defined for $\varepsilon \in [0, \varepsilon_3]$ and smooth for $\varepsilon \in (0, \varepsilon_3]$, and the image of Σ_3 is a thin strip lying exponentially close to $\mathcal{S}^{\mathrm{a}}_{\varepsilon,1} \cap \Sigma_1$, i.e., $\pi_3(\Sigma_3)$ is exponentially contracting with rate $\exp(-K_3/\varepsilon)$, for some $K_3 > 0$, in the f-direction while it is bounded in the e-direction.

Next, if the entry section Σ_1 is chosen such that $\Sigma_1 \supset \pi_3(\Sigma_3)$, Lemma 4 implies that there exists $\varepsilon_1 > 0$ such that the map π_1 is well-defined for any $\varepsilon \in [0, \varepsilon_1]$ and smooth for $\varepsilon \in (0, \varepsilon_1]$, and π_1 is an exponential contraction with rate $\exp(-K_1/\varepsilon)$ for some $K_1 > 0$. Finally, if the entry section Σ_2 is chosen such that $\Sigma_2 \supset \pi_1(\Sigma_1)$, Lemma 5 implies that there exists $\varepsilon_2 > 0$ such that the map π_2 is well-defined for any $\varepsilon \in [0, \varepsilon_2]$ and smooth for any $\varepsilon \in (0, \varepsilon_2]$, and further, π_2 is an exponential contraction with rate $\exp(-K_2/\varepsilon)$, for some $K_2 > 0$, such that $\Sigma_3 \supset \pi_2(\Sigma_2)$.

Denoting $\varepsilon_0 := \min\{\varepsilon_1, \varepsilon_2, \varepsilon_3\}$ and $K := \min\{K_1, K_2, K_3\}$, the map $\pi : \Sigma_3 \to \Sigma_3$ is well-defined for any $\varepsilon \in [0, \varepsilon_2]$, and smooth for $\varepsilon \in (0, \varepsilon_0]$. Further, based on the contracting properties of the maps π_i, $i = 1, 2, 3$, we conclude that $\pi(\Sigma_3) \subset \Sigma_3$ is contraction with rate $\exp(-K/\varepsilon)$. The Banach fixed-point theorem implies the existence of a unique fixed point for the map π, corresponding to the attracting periodic orbit of the system (9). Moreover, due to the last assertion of Lemmas 4, 5 and 6, the periodic orbit Γ_ε tends to the singular cycle Γ_0 as $\varepsilon \to 0$. This completes the proof.

4. Blow-up analysis

The slow-fast analysis that we have done in Section 3 does not explain the dynamics of system (9) close to the non-hyperbolic lines ℓ_1 and ℓ_2. As the segments ω_5 and ω_7 lie on these lines (see Fig. 9), we need a detailed analysis close to the lines ℓ_1 and ℓ_2, which is carried out in this section via the blow-up method [21,14,20]. To apply this, we extend system (9) by adding ε as a trivial dynamic variable and obtain

$$\begin{aligned}
\frac{df}{d\tau} &= [\gamma(1-f)(\varepsilon+2f) - 2fe(\varepsilon+1-f)]\, H_2^\varepsilon(c) H_3^\varepsilon(e),\\
\frac{dc}{d\tau} &= [8(1-c)f(\varepsilon+2c) - 4c(\varepsilon+2-2c)]\, H_1^\varepsilon(f) H_3^\varepsilon(e),\\
\frac{de}{d\tau} &= [8(1-e)c(\varepsilon+2e) - 4e(\varepsilon+2-2e)]\, H_1^\varepsilon(f) H_2^\varepsilon(c),\\
\frac{d\varepsilon}{d\tau} &= 0,
\end{aligned} \tag{35}$$

where $H_1^\varepsilon(f), H_2^\varepsilon(c)$ and $H_3^\varepsilon(e)$ are defined in (7). Note that for the extended system (35), the lines $\ell_1 \times \{0\}$ and $\ell_2 \times \{0\}$ are sets of equilibria. Due to the fact that the linearization of (35) around these lines has

quadruple zero eigenvalues, system (35) is very degenerate close to $\ell_1 \times \{0\}$ and $\ell_2 \times \{0\}$. To resolve these degeneracies, we use the blow-up method, given in next subsections.

4.1. Blow-up of the non-hyperbolic line $\ell_1 \times \{0\}$

The blow-up of the non-hyperbolic line $\ell_1 \times \{0\}$ is presented in this subsection. To this end, we transform the non-hyperbolic line of steady states $\ell_1 \times \{0\}$ by

$$f = r\bar{f}, \qquad c = r\bar{c}, \qquad \varepsilon = r\bar{\varepsilon}, \qquad e = \bar{e}, \tag{36}$$

where $\bar{f}^2 + \bar{c}^2 + \bar{\varepsilon}^2 = 1$ and $r \geq 0$. Note that since $(f, c, e) \in \mathcal{Q}$, we may further assume that $\bar{f}, \bar{c} \geq 0$ and $\bar{e} \in [0, 1]$. Since all weights are equal to 1 in (36), this is a homogeneous blow-up. For fixed $\bar{e}$, each point $(0, 0, \bar{e})$ is blown-up to a sphere $\mathbb{S}^2$, and the line $\ell_1 \times \{0\}$ is blown-up to a cylinder $\mathbb{S}^2 \times [0, 1]$, see Fig. 10.

For the analysis of system (35) near the line $\ell_1 \times \{0\}$, we define three charts K_1, K_2 and K_3 by setting $\bar{c} = 1$, $\bar{\varepsilon} = 1$, and $\bar{f} = 1$ in (36), respectively:

$$K_1: \quad f = r_1 f_1, \qquad c = r_1, \qquad \varepsilon = r_1\varepsilon_1, \qquad e = e_1, \tag{37}$$

$$K_2: \quad f = r_2 f_2, \qquad c = r_2 c_2, \qquad \varepsilon = r_2, \qquad e = e_2, \tag{38}$$

$$K_3: \quad f = r_3, \qquad c = r_3 c_3, \qquad \varepsilon = r_3\varepsilon_3, \qquad e = e_3. \tag{39}$$

The changes of coordinates for the charts K_1 to K_2, and K_2 to K_3 in the blown-up space are given in the following lemma.

Lemma 7. *The changes of coordinates K_1 to K_2, and K_2 to K_3 are given by*

$$\kappa_{12}: \quad f_2 = \frac{f_1}{\varepsilon_1}, \qquad c_2 = \frac{1}{\varepsilon_1}, \qquad \varepsilon_2 = r_1\varepsilon_1, \qquad e_2 = e_1, \qquad \varepsilon_1 > 0, \tag{40}$$

$$\kappa_{23}: \quad r_3 = r_2 f_2, \qquad c_3 = \frac{c_2}{f_2}, \qquad \varepsilon_3 = \frac{1}{f_2}, \qquad e_3 = e_2, \qquad f_2 > 0. \tag{41}$$

The goal of this subsection is to construct the transition map $\pi_1 : \Sigma_1 \to \Sigma_2$, defined in (31), and prove Lemma 4. Before going into the details, let us briefly describe our approach. We describe the transition map $\pi_1 : \Sigma_1 \to \Sigma_2$ via an equivalent one in the blown-up space. More specifically we define

$$\pi_1 := \Phi \circ \bar{\pi}_1 \circ \Phi^{-1}, \tag{42}$$

where

$$\bar{\pi}_1 := \Pi_3 \circ \kappa_{23} \circ \Pi_2 \circ \kappa_{12} \circ \Pi_1,$$

and $\Phi : \mathbb{S}^2 \times [0, 1] \times [0, r_0) \to \mathbb{R}^4$ is the cylindrical blow-up defined by (36), the maps Π_i are local transitions induced by the blown-up vector fields which are detailed below, and κ_{12} and κ_{23} denote the changes of coordinates, given in Lemma 7. $\bar{\pi}_1$ is the transition map in the blown-up space and due to the fact that Φ is a diffeomorphism, it is equivalent to π_1. A schematic of the problem at hand is shown in Fig. 10.

The left picture in Fig. 10 illustrates the critically manifolds $\mathcal{S}^{\mathrm{a}}_{0,1}$ and $\mathcal{S}^{\mathrm{a}}_{0,2}$, and the corresponding flows in blue. The non-hyperbolic line ℓ_1 is shown in orange. For $e > \gamma$, the reduced flows on both critically manifolds approach the line ℓ_1. At the point on the line ℓ_1 with $e = \gamma$, a transition from $\mathcal{S}^{\mathrm{a}}_{0,1}$ to $\mathcal{S}^{\mathrm{a}}_{0,2}$ is possible as indicated in the figure. The right picture in Fig. 10 schematically shows the configuration in the blown-up space. The cylinder corresponding to $r = 0$ is show in orange. The part of the phase space

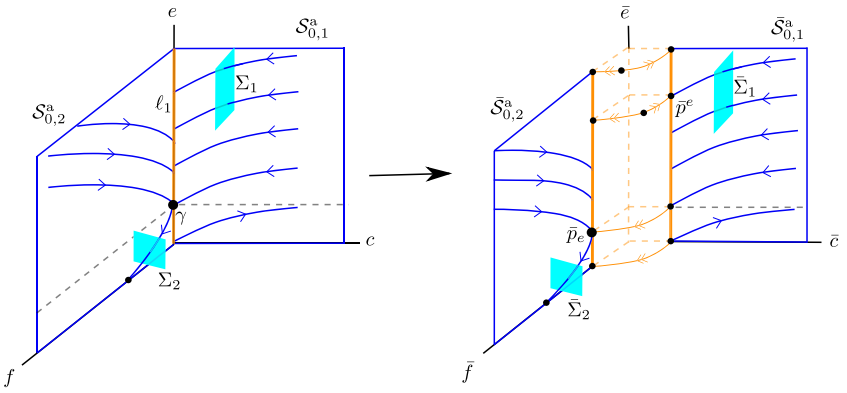

Fig. 10. The left figure shows the dynamics close to the non-hyperbolic line ℓ_1. The right figure shows the corresponding dynamics in the blown-up space.

corresponding to $\bar{\varepsilon} = 0$ and $r > 0$ are shown outside of the cylinder. Here we recover the layer problem, the critically manifolds, and the reduced flows in $\bar{\mathcal{S}}^a_{0,1}$ and $\bar{\mathcal{S}}^a_{0,2}$. In the blown-up space, the manifolds $\mathcal{S}^a_{0,1}$ and $\mathcal{S}^a_{0,2}$ are separated and hence gained hyperbolicity, in particular they are attractive, as indicated below in Fig. 11a. All these assertions will be proven in this section.

Roughly speaking, in chart K_1 we continue the attracting slow manifold $\bar{\mathcal{S}}^a_{0,1}$ onto the cylinder. Chart K_2 is used to track the flow across the cylinder. The exit of the flow from the cylinder and its transition to $\bar{\mathcal{S}}^a_{0,2}$ is studied in chart K_3, see Figs. 10 and 15. The detailed analysis of the maps Π_i introduced in (42), is given in the forthcoming subsections.

4.1.1. Analysis in chart K_1

After substituting (37) into (35) and dividing out all the equations by the common factor r_1, the equations governing the dynamics in chart K_1 are given by

$$\begin{aligned} f_1' &= -4f_1\Gamma_1 G_{11} + [\gamma(1-r_1f_1)(\varepsilon_1+2f_1) - 2f_1e_1(r_1\varepsilon_1+1-r_1f_1)]G_{12},\\ r_1' &= 4r_1\Gamma_1 G_{11},\\ e_1' &= 4r_1[2r_1(1-e_1)(r_1\varepsilon_1+2e_1) - e_1(r_1\varepsilon_1+2-2e_1)]G_{13},\\ \varepsilon_1' &= -4\varepsilon_1[2r_1f_1(1-r_1)(\varepsilon_1+2) - (r_1\varepsilon_1+2-2r_1)]G_{11}, \end{aligned} \tag{43}$$

where we denote

$$\begin{aligned} \Gamma_1 &:= [2r_1f_1(1-r_1)(\varepsilon_1+2) - (r_1\varepsilon_1+2-2r_1)],\\ G_{11} &:= (r_1\varepsilon_1+1-r_1f_1)(r_1\varepsilon_1+2-2e_1)(\varepsilon+2f_1)(r_1\varepsilon_1+2e_1),\\ G_{12} &:= (r_1\varepsilon_1+2-2r_1)(r_1\varepsilon_1+2-2e_1)(\varepsilon_1+2)(r_1\varepsilon_1+2e_1),\\ G_{13} &:= (r_1\varepsilon_1+1-r_1f_1)(r_1\varepsilon_1+2-2r_1)(\varepsilon_1+2f_1)(\varepsilon_1+2). \end{aligned} \tag{44}$$

From (43) it is clear that the planes $r_1 = 0$ and $\varepsilon_1 = 0$ are invariant. Hence, we consider the following cases:

1. $r_1 = \varepsilon_1 = 0$: in this case, the dynamics (43) is simplified to

$$\begin{aligned} e_1' &= 0,\\ f_1' &= 32f_1e_1(1-e_1)[2f_1+\gamma-e_1]. \end{aligned} \tag{45}$$

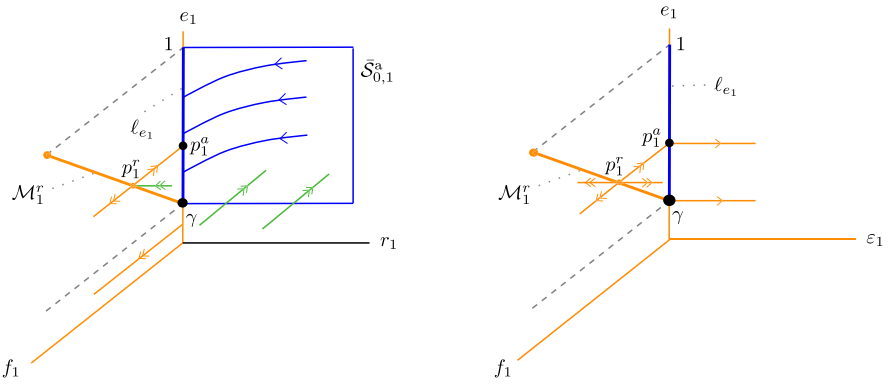

(a) Dynamics of (43) restricted to $\varepsilon_1 = 0$. (b) Dynamics of (43) restricted to $r_1 = 0$.

Fig. 11. Dynamics of (43) restricted to invariant subspaces.

For fixed e, the equilibria of the system (45) are the attracting point $p_1^a = (f_1, r_1, e_1, \varepsilon_1) = (0, 0, e_1, 0)$, and the repelling point $p_1^r = (f_1, r_1, e_1, \varepsilon_1) = (\frac{e_1-\gamma}{2}, 0, e_1, 0)$. Note that the two hyperbolic points p_1^a and p_1^r intersect at the non-hyperbolic point $(f_1, r_1, e_1, \varepsilon_1) = (0, 0, \gamma, 0)$, see Fig. 11a.

2. $\varepsilon_1 = 0$: in this case, the dynamics (43) is represented by

$$\begin{aligned} f_1' &= 32 f_1 e_1 (1-e_1)(1-r_1)(1-r_1 f_1)[(\gamma - e_1) - 2f_1(2r_1 f_1 - 1)], \\ r_1' &= 64 r_1 f_1 e_1 (1-e_1)(1-r_1)(1-r_1 f_1)[2r_1 f_1 - 1], \\ e_1' &= 64 r_1 f_1 e_1 (1-e_1)(1-r_1)(1-r_1 f_1)[2r_1 - 1]. \end{aligned} \tag{46}$$

From (46), one concludes that the plane $f_1 = 0$ is the plane of equilibria which is denoted by $\bar{\mathcal{S}}^{\mathrm{a}}_{0,1}$, see Fig. 11a. The non-zero eigenvalue along $\bar{\mathcal{S}}^{\mathrm{a}}_{0,1}$ is given by $\lambda = 32 e_1(1-e_1)(1-r_1)(\gamma - e_1)$. For $0 \le r_1 < 1$ and $e_1 > \gamma$, the plane $\bar{\mathcal{S}}^{\mathrm{a}}_{0,1}$ is attracting. As the e_1-axis is a part of $\bar{\mathcal{S}}^{\mathrm{a}}_{0,1}$, we denote that part of the e_1-axis that $\gamma \le e_1 \le 1$ by ℓ_{e_1}. We also have another curve of equilibria which is defined by $r_1 = 0$, and $f_1 = \frac{e_1-\gamma}{2}$, denoted by $\mathcal{M}_1^r$, see Fig. 11a. This curve of equilibria is of saddle-type with the eigenvalues $\lambda = \pm 32 e_1(e_1 - 1)(e_1 - \gamma)$. Note that we have recovered the information of the previous case here.

3. $r_1 = 0$: in this case, the dynamics (43) is represented by

$$\begin{aligned} e_1' &= 0, \\ f_1' &= 8 e_1 (1-e_1)[(\varepsilon_1 + 2)(\gamma(\varepsilon_1 + 2f_1) - 2f_1 e_1) + 4f_1(\varepsilon_1 + 2f_1)], \\ \varepsilon_1' &= 32 e_1 \varepsilon_1 (1-e_1)(\varepsilon_1 + 2f_1). \end{aligned} \tag{47}$$

By setting $\varepsilon_1 = 0$, we again have the line ℓ_{e_1} and the curve $\mathcal{M}_1^r$. The Jacobian matrix at a point in ℓ_{e_1} has two eigenvalues: one zero and the other one is $\lambda = 32 e_1(1-e_1)(\gamma - e_1)$. So the line ℓ_{e_1} is attracting when $e > \gamma$. As in this case we have two zero eigenvalues, it implies that there exists a two-dimensional center manifold, namely, $\mathcal{C}_{a,1}$.

Remark 14. In chart K_1, the most important role is played by the two-dimensional center manifold $\mathcal{C}_{a,1}$, see Lemma 9. In fact, this is the continuation of the critical manifold $\bar{\mathcal{S}}^{\mathrm{a}}_{0,1}$.

We summarize the analysis performed in this subsection in the following lemmas.

Lemma 8. *System (43) has the following manifolds of equilibria:*

1. *The plane $\bar{\mathcal{S}}^{a}_{0,1}$ which includes the line ℓ_{e_1},*

2. $\mathcal{M}_1^r = \{(f_1, r_1, e_1, \varepsilon_1) \mid f_1 = \frac{e_1-\gamma}{2},\ r_1 = 0,\ e_1 \in [\gamma, 1],\ \varepsilon_1 = 0\}$.

Lemma 9. *The following properties hold for system (43):*

1. *The linearization of (43) along $\bar{\mathcal{S}}_{0,1}^a$ has three zero eigenvalues, and the nonzero eigenvalue $\lambda = 32e_1(1-e_1)(1-r_1)(\gamma-e_1)$, which for $r_1 = 0$ corresponds to the flow in the invariant plane (f_1, e_1).*
2. *There exists a three-dimensional center manifold $\mathcal{W}_{a,1}^c$ of the line ℓ_{e_1} which contains the plane of equilibria $\bar{\mathcal{S}}_{0,1}^a$ and the two-dimensional center manifold $\mathcal{C}_{a,1}$. The manifold $\mathcal{W}_{a,1}^c$ is attracting, and in the set D_1, defined by*

$$D_1 := \{(f_1, r_1, e_1, \varepsilon_1) \mid 0 \le r_1 \le \delta_1,\ e_1 \in I_1,\ 0 \le \varepsilon_1 \le \alpha_1\},$$

is given by the graph

$$f_1 = h_{a,1}(r_1, e_1, \varepsilon_1),$$

where I_1 is a suitable interval, and $\alpha_1, \delta_1 > 0$ are sufficiently small. For the particular point $p_{a,1} \in \ell_{e_1}$ where $e^0 \in I_1$, the function $h_{a,1}(r_1, e^0, \varepsilon_1)$ has the expansion

$$h_{a,1}(r_1, e^0, \varepsilon_1) = \frac{\gamma}{2(e^0-\gamma)}\varepsilon_1 + O(\varepsilon_1^2). \tag{48}$$

3. *There exists $K > 0$ such that the orbits that are near the center manifold $\mathcal{W}_{a,1}^c$ are attracted to $\mathcal{W}_{a,1}^c$ by an exponential rate of order $O(\exp(-Kt_1))$.*

Proof. A straightforward calculation shows the first claim. Due to the fact that the linearization of (43) along $\bar{\mathcal{S}}_{0,1}^a$ has three zero eigenvalues, there exists [2,13] an attracting three-dimensional center manifold $\mathcal{W}_{a,1}^c$ at the point $p_{a,1}$. To derive equation (48), we first expand f_1 to the first order of variables r_1, e_1 and ε_1, and then plug into (43). By comparing the coefficients of r_1, e_1 and ε_1, equation (48) is obtained. The last claim is proven by the center manifold theory applied at the point $p_{a,1}$. □

Remark 15. The attracting center manifold $\mathcal{W}_{a,1}^c$ recovers parts of the slow manifold $\mathcal{S}_{\varepsilon,1}^a$ away form the line ℓ_1, and extends it into an $O(\varepsilon)$ neighborhood of ℓ_1. The slow manifold $\mathcal{S}_{\varepsilon,1}^a$ is obtained as a section $\varepsilon = constant$ of $\mathcal{W}_{a,1}^c$. In chart K_1, this center manifold is given by the graph (48).

Note that in chart K_1, our goal is to understand the dynamics (43) close to the center manifold $\mathcal{W}_{a,1}^c$, which corresponds to a sufficiently small neighborhood of the slow manifold $\bar{\mathcal{S}}_{0,1}^a$. Assume that $\delta_1, \alpha_1, \beta_1 > 0$ are small constants. Let us define the sections

$$\begin{aligned}
\Delta_1^{in} &:= \{(f_1, r_1, e_1, \varepsilon_1) \mid (f_1, r_1, e_1, \varepsilon_1) \in D_1,\ r_1 = \delta_1\},\\
\Delta_1^{out} &:= \{(f_1, r_1, e_1, \varepsilon_1) \mid (f_1, r_1, e_1, \varepsilon_1) \in D_1,\ \varepsilon_1 = \alpha_1\},\\
R_1^{in} &:= \{(f_1, r_1, e_1, \varepsilon_1) \mid (f_1, r_1, e_1, \varepsilon_1) \in D_1,\ r_1 = \delta_1, |f_1| \le \beta_1\}.
\end{aligned} \tag{49}$$

Note that by the way we have defined Δ_1^{in}, we in fact have $\Delta_1^{in} = \bar{\Sigma}_1 := \Phi^{-1}(\Sigma_1 \times \{[0, \rho_1]\})$ for some $\rho_1 > 0$, see Fig. 10. Furthermore, the constants $\delta_1, \alpha_1, \beta_1$ are chosen such that $R_1^{in} \subset \Delta_1^{in}$, and the intersection of the center manifold $\mathcal{W}_{a,1}^c$ with Δ_1^{in} lies in R_1^{in}, i.e., $\mathcal{W}_{a,1}^c \cap \Delta_1^{in} \subset R_1^{in}$.

Let us denote Π_1 as the transition map from Δ_1^{in} to Δ_1^{out}, induced by the flow of (43). In order to construct map Π_1, we reduce system (43) to the center manifold $\mathcal{W}_{a,1}^c$ and analyze the system based on the dynamics on $\mathcal{W}_{a,1}^c$. To this end, by substituting (48) into (43) and rescaling time, the flow of the center manifold is given by

$$\begin{aligned} r_1' &= -r_1, \\ e_1' &= -\frac{1}{2}[O(r_1) + O(r_1\varepsilon_1)], \\ \varepsilon_1' &= \varepsilon_1, \end{aligned} \tag{50}$$

where the derivative is with respect to the new timescale, namely, t_1. Now let us consider a solution of (50), namely, $(r_1(t_1), e_1(t_1), \varepsilon_1(t_1))$ which satisfies the following conditions:

$$\begin{aligned} r_1(0) &= \delta_1, & r_1(T^{out}) &= r_1^{out}, \\ e_1(0) &= e_1^{in}, & e_1(T^{out}) &= e_1^{out}, \\ \varepsilon_1(0) &= \varepsilon_1^{in}, & \varepsilon_1(T^{out}) &= \alpha_1. \end{aligned} \tag{51}$$

From equation $\varepsilon_1' = \varepsilon_1$ with the conditions $\varepsilon_1(0) = \varepsilon_1^{in}$ and $\varepsilon_1(T^{out}) = \alpha_1$, we can calculate the time that $(r_1(t_1), e_1(t_1), \varepsilon_1(t_1))$ needs to travel from Δ_1^{in} to Δ_1^{out}, which is given by

$$T^{out} = \ln \frac{\alpha_1}{\varepsilon_1^{in}}. \tag{52}$$

Since $e_1' = -\frac{1}{2}[O(r_1) + O(r_1\varepsilon_1)]$ with $e_1(T^{in}) = e_1^{in}$, we can estimate the time evolution of $e_1(t_1)$, which is given by

$$e_1(t_1) = \frac{r_1^{in}}{2}\left[\exp(-t_1) - 1 - t_1\varepsilon_1^{in}\right] + e_1^{in}, \qquad 0 \le t_1 \le T^{out}. \tag{53}$$

Hence, in view of (52), one has

$$e_1(T^{out}) = e_1^{out} := \frac{r_1^{in}}{2}\left(\frac{\varepsilon_1^{in}}{\alpha_1} - 1 - \varepsilon_1^{in}\ln\frac{\alpha_1}{\varepsilon_1^{in}}\right) + e_1^{in}. \tag{54}$$

We summarize the analysis performed for chart K_1 in the following theorem.

Theorem 3. *For system (43) with sufficiently small $\delta_1, \alpha_1, \beta_1$ and $R_1^{in} \subset \Delta_1^{in}$, the transition map $\Pi_1 : R_1^{in} \to \Delta_1^{out}$ is well-defined and has the following properties:*

1. *$\Pi_1(R_1^{in}) \subset \Delta_1^{out}$ is a three-dimensional wedge-like region in Δ_1^{out}.*
2. *The transition map Π_1 is given by*

$$\Pi_1\begin{pmatrix} f_1 \\ \delta_1 \\ e_1 \\ \varepsilon_1 \end{pmatrix} = \begin{pmatrix} h_{a,1}(\frac{\delta_1}{\alpha_1}\varepsilon_1, e_1^{out}, \alpha_1) + \Psi(\delta_1, e_1, \varepsilon_1) \\ \frac{\delta_1}{\alpha_1}\varepsilon_1 \\ e_1^{out} \\ \alpha_1 \end{pmatrix},$$

where e_1^{out} is given in (54), $\Psi(\cdot)$ is an exponentially small function, and $h_{a,1}(\cdot)$ is of order $O(\varepsilon_1)$, due to (48).

4.1.2. Analysis in chart K_2

After substituting (38) into (35) and dividing out all the equations by the common factor r_2, the equations governing the dynamics in chart K_2 are given by

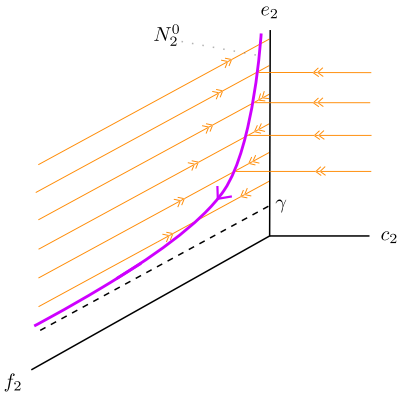

Fig. 12. Fully attracting critical manifold N_2^0 in purple, and the slow and fast dynamics in chart K_2.

$$\begin{aligned} f_2' &= 8e_2\left[\gamma(1+2f_2)-2f_2e_2\right](1-e_2)(1+2c_2)+O(\varepsilon),\\ c_2' &= -32c_2e_2(1-e_2)(1+2f_2)+O(\varepsilon),\\ e_2' &= -16\varepsilon e_2(1-2e_2)(1+2f_2)(1+2c_2)+O(\varepsilon^2),\\ \varepsilon' &= 0. \end{aligned} \tag{55}$$

Due to the fact that $r_2=\varepsilon$ in chart K_2, we have presented (55) in terms of ε. Note that since $r_2'=\varepsilon'=0$, system (55) is a family of three-dimensional vector fields which are parametrized by ε. Moreover, system (55) is a slow-fast system in the standard form, i.e., e_2 is the slow variable, and f_2 and c_2 are the fast variables. Since the differentiation $'$ in (55) is with respect to the fast time variable, namely τ_2, by transforming it to the slow time variable we have $t_2=\varepsilon\tau_2$, and hence

$$\begin{aligned} \varepsilon\dot{f}_2 &= 8e_2\left[\gamma(1+2f_2)-2f_2e_2\right](1-e_2)(1+2c_2)+O(\varepsilon),\\ \varepsilon\dot{c}_2 &= -32c_2e_2(1-e_2)(1+2f_2)+O(\varepsilon),\\ \dot{e}_2 &= -16e_2(1-2e_2)(1+2f_2)(1+2c_2)+O(\varepsilon), \end{aligned} \tag{56}$$

where the derivative is with respect to t_2. Now by setting $\varepsilon=0$ in (55) we obtain the corresponding layer problem

$$\begin{aligned} f_2' &= 8e_2\left[\gamma(1+2f_2)-2f_2e_2\right](1-e_2)(1+2c_2),\\ c_2' &= -32c_2e_2(1-e_2)(1+2f_2),\\ e_2' &= 0, \end{aligned} \tag{57}$$

which has the associated critical manifold $c_2=0$ and $f_2=\frac{\gamma}{2(e_2-\gamma)}$, denoted by N_2^0 (see Fig. 12). The Jacobian matrix corresponding to (57) along this critical manifold has the eigenvalues

$$\lambda_{21}=-16e_2(1-e_2)(e_2-\gamma), \qquad \lambda_{22}=\frac{32e_2^2(e_2-1)}{(e_2-\gamma)}. \tag{58}$$

As it is clear form (58), the critical manifold restricted to $e_2\in(\gamma,1)$ is normally hyperbolic, and specially, is fully attracting since both of the eigenvalues are negative. As e_2 approaches γ from above, f_2 develops a singularity along N_2^0. Thus, the behavior of N_2^0 as $e\to\gamma$ has to be studied in chart K_3. Using Fenichel theory and the dynamics in chart K_2 for $\varepsilon=0$, one is able to describe the dynamics for $0<\varepsilon\ll 1$ in this chart, i.e., there exists a slow manifold N_2^ε which is the ε-perturbation of N_2^0. We summarize the properties of the critical manifold of chart K_2 in the following lemma.

Lemma 10. *The critical manifold*

$$N_2^0 = \{(f_2, c_2, e_2) \mid f_2 = \frac{\gamma}{2(e_2-\gamma)},\ c_2 = 0,\ e_2 \in I_2^0\}, \tag{59}$$

is fully attracting, where I_2^0 is a compact subset of the interval $(\gamma, 1)$. Moreover, there exists $\varepsilon_0 > 0$ such that for any $\varepsilon \in (0, \varepsilon_0)$, there exists a smooth locally invariant attracting one-dimensional slow manifold N_2^ε, which is $O(\varepsilon)$-close to N_2^0, with the slow flow

$$\dot{e}_2 = -4e_2(\varepsilon + 2 - 2e_2)(\varepsilon + 1 - \varepsilon f_2)(\varepsilon + 2)(1 + 2f_2). \tag{60}$$

Note that e_2 is decreasing along N_2^ε, see Fig. 12. Now, we construct the transition map Π_2. For this let us define the sections

$$\Delta_2^{in} := \{(f_2, c_2, e_2, \varepsilon) \mid f_2 \in [0, \beta_2],\ c_2 = \frac{1}{\alpha_1},\ e_2 \in I_2,\ \varepsilon \in [0, \alpha_2]\},$$
$$\Delta_2^{out} := \{(f_2, c_2, e_2, \varepsilon) \mid f_2 = \beta_2,\ c_2 \in [0, \frac{1}{\alpha_1}],\ e_2 \in I_2,\ \varepsilon \in [0, \alpha_2]\},$$

where δ_1 is small, $\beta_2 = \frac{\beta_1}{\alpha_1}$, $\alpha_2 = \delta_1\alpha_1$, and I_2 is a suitable interval. Note that $\Delta_2^{in} = \kappa_{12}(\Delta_1^{out})$. Let us define the transition map from Δ_2^{in} to Δ_2^{out} as follows:

$$\Pi_2 : \Delta_2^{in} \to \Delta_2^{out}, \qquad (f_2^{in}, \frac{1}{\alpha_1}, e_2^{in}, \varepsilon) \mapsto (\beta_2, c_2^{out}, e_2^{out}, \varepsilon). \tag{61}$$

The map Π_2 is described by the Fenichel theory, i.e., all orbits starting from $(f_2^{in}, \frac{1}{\alpha_1}, e_2^{in}, \varepsilon)$ are attracted by the slow manifold N_2^ε, follow the slow manifold along N_2^ε, and then after some time intersect the section Δ_2^{out} transversally.

Remark 16. In the limit $\varepsilon = 0$, the map Π_2 is defined by first projecting $(f_2, e_2) \in \Delta_2^{in}$ onto N_2^0 along the stable foliation, and then by following the slow flow (60).

We summarize the analysis performed in chart K_2 in the following lemma.

Lemma 11. *For small $\alpha_1 > 0$, there exists a sufficiently small $\alpha_2 > 0$ such that the transition map Π_2, defined in (61), is well-defined. Moreover, for ε = constant, Π_2 is contracting with the contraction rate $\exp(-K/\varepsilon)$ for some $K > 0$.*

Proof. The transition map $\Pi_2 : \Delta_2^{in} \to \Delta_2^{out}$ is described by Fenichel theory, i.e., all orbits starting from Δ_2^{in} are attracted by the slow manifold N_2^ε, with a contraction rate $\exp(-K/\varepsilon)$ for some $K > 0$, and after some time they reach the section Δ_2^{out}. □

Remark 17. The slow manifold N_2^ε corresponds to the perturbation of N_2^0 when ε = *constant*. The family of all such manifolds is denoted by $\mathcal{N}_2$.

4.1.3. Analysis in chart K_3

Solutions in chart K_2 which reach the section Δ_2^{out} must be continued in chart K_3. For this reason, we continue our analysis in chart K_3. After substituting (39) into (35) and dividing out all the equations by the common factor r_3, the equations governing the dynamics in chart K_3 are given by

$$
\begin{aligned}
r_3' &= r_3\Gamma_3 G_{31},\\
c_3' &= -c_3\Gamma_3 G_{31} + \left[8r_3(1-r_3c_3)(\varepsilon_3+2c_3) - 4c_3(r_3\varepsilon_3+2-2r_3c_3)\right] G_{32},\\
e_3' &= r_3\left[8r_3c_3(1-e_3)(r_3\varepsilon_3+2e_3) - 4e_3(r_3\varepsilon_3+2-2e_3)\right] G_{33},\\
\varepsilon_3' &= -\varepsilon_3\Gamma_3 G_{31},
\end{aligned}
\tag{62}
$$

where we denote

$$
\begin{aligned}
\Gamma_3 &:= \left[\gamma(1-r_3)(\varepsilon_3+2) - 2e_3(r_3\varepsilon_3+1-r_3)\right],\\
G_{31} &:= (r_3\varepsilon_3+2-2r_3c_3)(\varepsilon_3+2c_3)(r_3\varepsilon_3+2-2e_3)(r_3\varepsilon_3+2e_3),\\
G_{32} &:= (r_3\varepsilon_3+1-r_3)(\varepsilon_3+2)(r_3\varepsilon_3+2-2e_3)(r_3\varepsilon_3+2e_3),\\
G_{33} &:= (r_3\varepsilon_3+1-r_3)(\varepsilon_3+2)(r_3\varepsilon_3+2-2r_3c_3)(\varepsilon_3+2c_3).
\end{aligned}
$$

System (62) has three invariant subspaces, namely, $r_3 = 0$, $\varepsilon_3 = 0$ and their intersection. Recall that by definition $e = e_3$ and thus $0 < e_3 < 1$.

1. $r_3 = \varepsilon_3 = 0$: in this case the dynamics is governed by

$$
\begin{aligned}
c_3' &= -32c_3e_3(1-e_3)[2+c_3(\gamma-e_3)]\\
e_3' &= 0.
\end{aligned}
\tag{63}
$$

When $e_3 > \gamma$ the equilibria of the system are $p_3^a = (r_3, c_3, e_3, \varepsilon_3) = (0, 0, e_3, 0)$ and $p_3^r = (r_3, c_3, e_3, \varepsilon_3) = (0, \frac{2}{e_3-\gamma}, e_3, 0)$. Note that the point p_3^a is attracting for the flow in the plane (c_3, e_3), while the point p_3^r is repelling.

Remark 18. Note that when $e_3 \to \gamma$, the point $p_3^r \to \infty$ and is not visible any more in the chart K_3, see Fig. 13a.

2. $\varepsilon_3 = 0$ and $r_3 \geq 0$: In the invariant plane $\varepsilon_3 = 0$, the dynamics is governed by

$$
\begin{aligned}
r_3' &= r_3c_3\left[\gamma - e_3\right]V(r_3, c_3, e_3),\\
c_3' &= c_3\left[(4r_3-2) - c_3(\gamma-e_3)\right]V(r_3, c_3, e_3),\\
e_3' &= 2r_3c_3\left[(2r_3c_3-1)\right]V(r_3, c_3, e_3),
\end{aligned}
\tag{64}
$$

where $V(r_3, c_3, e_3) = 32e_3(1-r_3)(1-e_3)(1-r_3c_3)$. Recall that $c = r_3c_3$ and therefore $V(r_3, c_3, e_3) > 0$. The equilibria of the system are the plane $c_3 = 0$, denoted by $\bar{\mathcal{S}}_{0,2}$, and the curve of equilibria given by $c_3 = \frac{2}{e_3-\gamma}$, denoted by $\mathcal{M}_3^r$. The change of stability of the points in $\bar{\mathcal{S}}_{0,2}$ occurs at $r_3 = 0.5$, i.e., for $r_3 < 0.5$ the points are attracting, while for $r_3 > 0.5$ they are repelling. We denote the attracting part of $\bar{\mathcal{S}}_{0,2}$ by $\bar{\mathcal{S}}_{0,2}^{\mathrm{a}}$. The e_3-axis, which we denote by ℓ_{e_3}, is a boundary of $\bar{\mathcal{S}}_{0,2}^{\mathrm{a}}$, which is a line of equilibria.

3. $r_3 = 0$ and $\varepsilon_3 \geq 0$: In the invariant plane $r_3 = 0$, the dynamics is governed by

$$
\begin{aligned}
e_3' &= 0,\\
c_3' &= -8c_3e_3(1-e_3)\left[(\gamma(\varepsilon_3+2) - 2e_3)(\varepsilon_3+2c_3) + 4(\varepsilon_3+2)\right],\\
\varepsilon_3' &= -8\varepsilon_3e_3(1-e_3)\left[\gamma(\varepsilon_3+2) - 2e_3\right](\varepsilon_3+2c_3).
\end{aligned}
\tag{65}
$$

The equilibria of the system are the planes $c_3 = 0$, and the line $\varepsilon_3 = \frac{2(e_3-\gamma)}{\gamma}$, denoted by N_3^0. The Jacobian of (65) along the curve N_3^0 has the eigenvalues

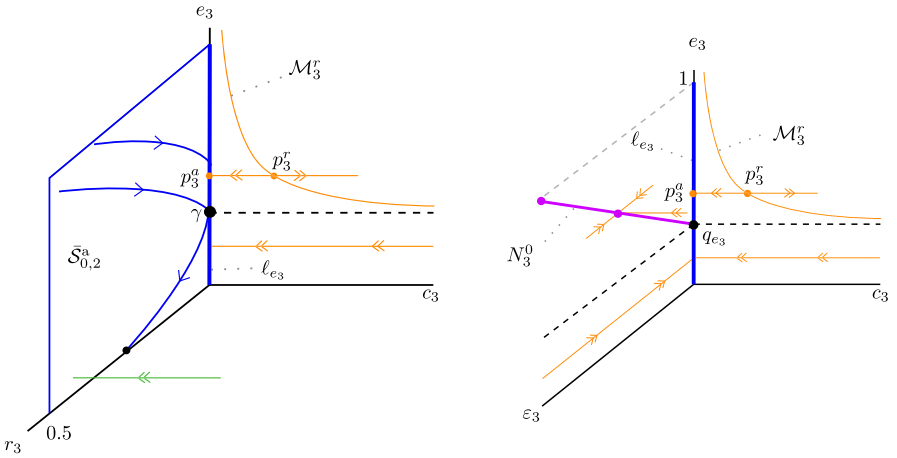

(a) Dynamics of (62) restricted to $\varepsilon_3 = 0$. (b) Dynamics of (62) restricted to $r_3 = 0$.

Fig. 13. Dynamics of system (62) restricted to invariant subspaces.

$$\lambda_{31} = -64e_3(c_3+1)(1-e_3), \qquad \lambda_{32} = -8\gamma\varepsilon_3 e_3(1-e_3)(\varepsilon_3+2c_3), \tag{66}$$

and hence N_3^0 is fully attracting. In fact, N_3^0 is exactly the critical manifold N_2^0 that we found in chart K_2. In other words, N_3^0 is the image of N_2^0 under the transformation κ_{23}, defined in (41).

Remark 19. Note that the attracting manifold N_2^0 that is unbounded in chart K_2, is now bounded in chart K_3. So the behavior of the critical manifold that is not visible in chart K_2 when $e \to \gamma$, is now visible in chart K_3. For $e_3 = \gamma$, the critical manifold N_3^0 intersects the line ℓ_{e_3} at the non-hyperbolic point $q_{e_3} = (e_3, c_3, \varepsilon_3) = (\gamma, 0, 0)$.

We summarize the analysis of the invariant planes, performed in this subsection, in the following Lemma.

Lemma 12. *The following properties hold for system* (62)*:*

1. *The equilibria are the plane* $\bar{\mathcal{S}}_{0,2}$ *which intersects the line* ℓ_{e_3}*, and the following two one-dimensional manifolds*

$$\mathcal{M}_3^r = \{(r_3.c_3, e_3, \varepsilon_3) \mid r_3 = \varepsilon_3 = 0,\ e_3 \in (\gamma, 1),\ c_3 = \frac{2}{e_3-\gamma}\},$$
$$N_3^0 = \{(r_3.c_3, e_3, \varepsilon_3) \mid r_3 = c_3 = 0,\ e_3 \in [\gamma, 1),\ \varepsilon_3 = \frac{2(e_3-\gamma)}{\gamma}\}.$$

2. *For* $e_3 > \gamma$*, the equilibria of system* (62) *along* N_3^0 *have*
   (a) *a two-dimensional stable manifold corresponding to the negative eigenvalues given in* (66)*.*
   (b) *a two-dimensional center manifold corresponding to a double zero eigenvalue.*
3. *The linearization of the system in* $\bar{\mathcal{S}}_{0,2}$ *has a triple zero eigenvalue, and the eigenvalue* $\lambda = 64e_3(e_3-1)(r_3-1)(r_3-0.5)$ *changes its stability at* $r_3 = 0.5$*.*
4. *The linearization of system* (62) *at the steady states in the line* ℓ_{e_3} *has a stable eigenvalue* $\lambda = 64e_3(e_3-1)$*, and a triple zero eigenvalue. Moreover, there exists a three-dimensional center manifold* $\mathcal{W}^c_{a,\varepsilon}$ *at the point* $(r_3, c_3, e_3, \varepsilon_3) = (0, 0, e_3, 0) \in \ell_{e_3}$*. In chart* K_3 *close to the point* $e_3 = \gamma$*, the center manifold* $\mathcal{W}^c_{a,\varepsilon}$ *is given as the graph*

$$c_3 = r_3\varepsilon_3(1 + O(r_3\varepsilon_3)). \tag{67}$$

The main goal of chart K_3 is to analyze the behavior of the solutions of (62) close to the exit point $q_{e_3} \in \ell_{e_3}$. From our analysis in chart K_2, we know that there exists the family of attracting slow manifolds $\mathcal{N}_2$. This in chart K_3 is denoted by $\mathcal{N}_3$ which is the image of $\mathcal{N}_2$ under the transformation κ_{23}, i.e. $\mathcal{N}_3 = \kappa_{23}(\mathcal{N}_2)$. In order to know how $\mathcal{N}_3$ is continued close to the point q_{e_3}, we restrict the dynamics to the sets

$$D_3^{in} := \{(r_3, c_3, e_3, \varepsilon_3) \mid r_3 \in [0, \alpha_3], e_3 \in (\gamma, 1], \varepsilon_3 \in [0, \beta_3]\},$$
$$D_3^{out} := \{(r_3, c_3, e_3, \varepsilon_3) \mid r_3 \in [0, \alpha_3], e_3 \in [0, \gamma), \varepsilon_3 \in [0, \beta_3]\},$$

where $\alpha_3 = \alpha_2\beta_2$ and $\beta_3 = \frac{1}{\beta_2}$, due to the transformation κ_{23} defined in (41). Now we define the sections as follows

$$\Delta_3^{in} := \{(r_3, c_3, e_3, \varepsilon_3) \in D_3^{in} \mid \varepsilon_3 = \beta_3\},$$
$$\Delta_3^{out} := \{(r_3, c_3, e_3, \varepsilon_3) \in D_3^{out} \mid r_3 = \alpha_3\}.$$

Let us denote Π_3 as the transition map from Δ_3^{in} to Δ_3^{out}, induced by the flow of (62). In order to construct the map Π_3, we reduce system (62) to its center manifold, namely, $\mathcal{W}^c_{a,3}$ and analyze the system based on the dynamics on $\mathcal{W}^c_{a,3}$. This is done by substituting (67) into system (62), and rescaling time by dividing out the common factor

$$\left[r_3\varepsilon_3 + 2 - 2r_3^2\varepsilon_3(1 + O(r_3\varepsilon_3)\right]\left[\varepsilon_3 + 2r_3\varepsilon_3(1 + O(r_3\varepsilon_3)\right]. \tag{68}$$

The flow of the center manifold is given by

$$\begin{aligned} r_3' &= r_3 G_{34}, \\ e_3' &= r_3 G_{35}, \\ \varepsilon_3' &= -\varepsilon_3 G_{34}, \end{aligned} \tag{69}$$

where we denote

$$G_{34} := [\gamma(1 - r_3)(\varepsilon_3 + 2) - 2e_3(r_3\varepsilon_3 + 1 - r_3)]\,(r_3\varepsilon_3 + 2 - 2e_3)(r_3\varepsilon_3 + 2e_3),$$
$$G_{35} := \left[8r_3^2\varepsilon_3(1 + O(r_3\varepsilon_3))(1 - e_3)(r_3\varepsilon_3 + 2e_3) - 4e_3(r_3\varepsilon_3 + 2 - 2e_3)\right](r_3\varepsilon_3 + 1 - r_3)(\varepsilon_3 + 2).$$

It is clear from (69) that the planes $r_3 = 0$ and $\varepsilon_3 = 0$ are invariant. Setting $r_3 = 0$ in (69), one obtains

$$\begin{aligned} e_3' &= 0, \\ \varepsilon_3' &= -4\varepsilon_3 e_3(1 - e_3)[\gamma(\varepsilon_3 + 2) - 2e_3]. \end{aligned} \tag{70}$$

The equilibria of (69) are again the line ℓ_{e_3} and the manifold N_3^0. The Jacobian of (70) evaluated at the line ℓ_{e_3} has the eigenvalue $\lambda = 8e_3(1 - e_3)(e_3 - \gamma)$, showing that ℓ_{e_3} is repelling for $e_3 > \gamma$, while attracting for $e_3 < \gamma$. Moreover, the manifold N_3^0 is attracting for the flow in the plane $r_3 = 0$. The eigenvalue at the point $(r_3, e_3, \varepsilon_3) = (0, \gamma, 0) \in \ell_{e_3}$ is zero and hence this point is degenerate.

Setting $\varepsilon_3 = 0$ in system (69) results in

$$\begin{aligned} r_3' &= 8r_3e_3(1 - e_3)(1 - r_3)[\gamma - e_3], \\ e_3' &= -16r_3e_3(1 - e_3)(1 - r_3). \end{aligned} \tag{71}$$

In the plane $\varepsilon_3 = 0$, the line ℓ_{e_3} is attracting for $e_3 > \gamma$ while repelling for $e_3 < \gamma$.

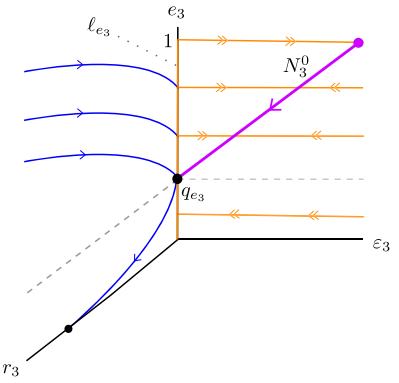

Fig. 14. Dynamics of the system (69); the attracting manifold N_3^0 in purple, and the nilpotent point q_{e_3} in black.

Remark 20. Note that the dynamics in the invariant plane $\varepsilon = 0$ corresponds to the reduced flow on S_a^2 in the original system.

Summarizing the analysis, we have the following lemma.

Lemma 13. *The following properties hold for system* (69)*:*

1. *The curve N_3^0 has a one dimensional stable manifold, and a two dimensional center manifold away from the point q_{e_3}.*
2. *The linearization of* (69) *at the points in ℓ_{e_3} is given by*

$$\begin{pmatrix} 8e_3(e_3-1)(e_3-\gamma) & 0 & 0 \\ 16e_3(e_3-1) & 0 & 0 \\ 0 & 0 & -8e_3(e_3-1)(e_3-\gamma) \end{pmatrix},$$

3. *The point q_{e_3} is nilpotent.*

As we already mentioned, our goal in chart K_3 is to describe the dynamics (62) close to the line ℓ_{e_3}, and especially at the point q_{e_3}. To this end, we defined the map $\Pi_3 : \Delta_3^{in} \to \Delta_3^{out}$ where Δ_3^{in} is transversal to N_3^0 for $e > \gamma$, while Δ_3^{out} is transversal to the slow manifold in the plane $\varepsilon_3 = 0$ for $e < \gamma$. From Lemma 13 we know that the point q_{e_3} is nilpotent. Thus, in order to describe the transition map Π_3 we need to blow-up the point q_{e_3}. For such a point, a similar analysis has been carried out in [18, Theorem 5.8], in view of which we have the following theorem.

Theorem 4. *Assume that $R_3 \subset \Delta_3^{in}$ is a small rectangle centered at the intersection point $N_3^0 \cap \Delta_3^{in}$. For sufficiently small α_3, the transition map $\Pi_3 : R_3 \to \Delta_3^{out}$ induced by the flow of* (69) *is well-defined and satisfies the following properties:*

1. *The continuation of $\mathcal{N}_3$ by the flow intersects the section Δ_3^{out} in a curve denoted by σ_3^{out}.*
2. *Restricted to the lines $r_3 = constant$ in R_3, the map is contracting with the rate $\exp(-K/r_3)$ for some $K > 0$.*
3. *The image $\Pi_3(R_3)$ is an exponentially thin wedge-like containing the curve σ_3^{out}.*

Finally, if we set $\alpha_3 = \delta_2$ (recall the definition of Σ_2) we actually have that $\Delta_3^{out} = \bar{\Sigma}_2 := \Phi^{-1}(\Sigma_2 \times \{[0, \rho_2]\})$ for some $\rho_2 > 0$.

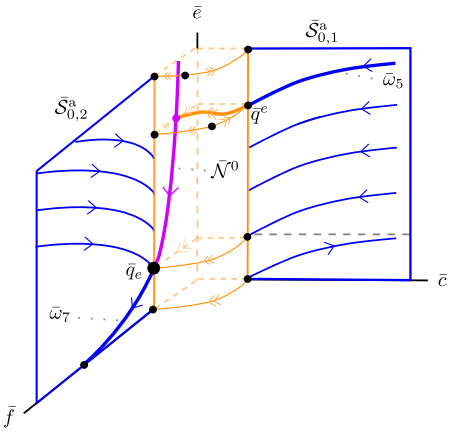

Fig. 15. Geometry of the blown-up space and the singular cycle close to the non-hyperbolic line ℓ_1, which is blown-up to the orange cylinder. The reduced flows in $\bar{\mathcal{S}}^{a}_{0,1}$ and $\bar{\mathcal{S}}^{a}_{0,1}$ are illustrated in blue. The thick orange manifold inside the cylinder corresponds to the three-dimensional center manifold in chart K_1. The attracting critical manifold in chart K_2 is shown in purple.

4.1.4. Properties of the blow-up of the non-hyperbolic line $\ell_1 \times \{0\}$ and proof of Lemma 4

In the above subsections, we have presented the detailed analysis of the blow-up of the non-hyperbolic line $\ell_1 \times \{0\}$ in charts K_1, K_2 and K_3, which has been summarized in Fig. 15. A summary of the analysis, carried out in such charts, is as follows. First of all, the critical manifolds $\mathcal{S}_{0,1}$ (i.e., $f = 0$) and $\mathcal{S}_{0,2}$ (i.e., $c = 0$) intersect in the non-hyperbolic line ℓ_1, which is replaced by the orange cylinder, see Figs. 10 and 15. Note that in Fig. 15, the orbits $\bar{\omega}_5$ and $\bar{\omega}_7$ in the blown-up space correspond to the orbits ω_5 and ω_7, respectively. The point at which $\bar{\omega}_5$ reaches the cylinder is denoted by $\bar{q}^e$, and the point at which $\bar{\omega}_7$ starts is denoted by $\bar{q}_e$. Starting from the section $\bar{\Sigma}_1$, the trajectory follows the orbit $\bar{\omega}_5$ on $\bar{f} = 0$ until it reaches the point $\bar{q}^e$. Our analysis in chart K_1 (Lemma 9) shows that there exists a three-dimensional attracting center manifold which is the continuation of the family of orbits (indexed by ε) of the attracting slow manifold $\mathcal{S}^{a}_{\varepsilon,1}$. This allows us to connect the family $\mathcal{S}^{a}_{\varepsilon,1}$ into the chart K_2 which is inside the cylinder (see the thick orange manifold from $\bar{q}^e$ to $\bar{\mathcal{N}}^0$ in Fig. 15). Our analysis in chart K_2 (Lemma 10) shows that the slow manifold N_2^0 is normally hyperbolic and stable. Therefore, the family $\mathcal{S}^{a}_{\varepsilon,1}$ is exponentially attracted by the slow manifold N_2^{ε}. Next, our analysis in chart K_3 shows that the unbounded critical manifold N_2^0 (see Figs. 12, 14) limits in the point q_{e_3}, which is exactly the point $\bar{q}_e$ in Fig. 15. Next, our analysis in chart K_3 (see Lemma 13 and Fig. 14) demonstrates that the unbounded critical manifold N_2^{ε} (see Figs. 12 and 14) limits at the point q_{e_3}, which is exactly the point $\bar{q}_e$ in Fig. 15. In addition, we have proven that the point q_{e_3} is degenerate, i.e., the linearization of the dynamics at q_{e_3} has a nonzero (stable) eigenvalue and a triple zero eigenvalue (see Lemma 13), which allows us to construct a three-dimensional center manifold at the point q_{e_3}. Now, by following the family $\mathcal{N}_2$ along such a center manifold, we conclude (Lemma 4) that the continuation of N_2^{ε} for a sufficiently small $\varepsilon > 0$ intersects the section $\bar{\Sigma}_2$ in a point, namely, $(\alpha_3, c_3(\varepsilon_3), e_3(\varepsilon_3), \varepsilon_3) \in \bar{\Sigma}_2$, for some $\varepsilon_3 \in [0, \beta_3]$, which is exponentially close to the slow manifold $\mathcal{S}^{a}_{\varepsilon,2}$. Note that the point $(\alpha_3, c_3(\varepsilon_3), e_3(\varepsilon_3), \varepsilon_3)$ converges to the point $q_2 := \Sigma_2 \cap \omega_7$ as $\varepsilon_3 \to 0$. All these analyses in charts K_1, K_2, and K_3 show that the transition map $\bar{\pi}_1 : \bar{\Sigma}_1 \to \bar{\Sigma}_2$ is well-defined for $\varepsilon \in [0, \varepsilon_0]$ and is smooth for $\varepsilon \in (0, \varepsilon_0]$, for some $\varepsilon_0 > 0$.

We are now ready to prove Lemma 4.

Proof of Lemma 4. The proof is carried out by constructing the map $\pi_1 : \Sigma_1 \to \Sigma_2$ for $\varepsilon > 0$ as

$$\pi_1 = \Phi \circ \bar{\pi}_1 \circ \Phi^{-1}, \tag{72}$$

where Φ is given by (36), Φ^{-1} is the corresponding blown-up transformation, and $\bar{\pi}_1 : \bar{\Sigma}_1 \to \bar{\Sigma}_2$ is a transition map which can equivalently be regarded as

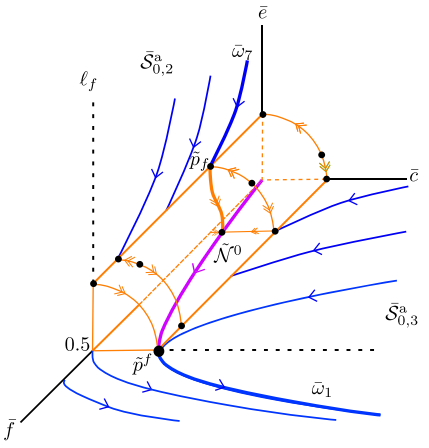

Fig. 16. Geometry of the blown-up space and the singular cycle close to the non-hyperbolic line ℓ_2, which is blown-up to the orange cylinder. The reduced flows in $\bar{\mathcal{S}}^{a}_{0,2}$ and $\bar{\mathcal{S}}^{a}_{0,3}$ are shown in blue. The thick orange manifold inside the cylinder corresponds to the three-dimensional center manifold in chart $\tilde{K}_1$. The attracting critical manifold in chart $\tilde{K}_2$ is illustrated in purple.

$$\bar{\pi}_1(\bar{\Sigma}_1) = \Pi_3 \circ \kappa_{23} \circ \Pi_2 \circ \kappa_{12} \circ \Pi_1(\bar{\Sigma}_1) \subset \bar{\Sigma}_2 \tag{73}$$

The proof is based on the corresponding transition map $\bar{\pi}_1 : \bar{\Sigma}_1 \to \bar{\Sigma}_2$ in the blown-up space and interpreting the result for fixed $\varepsilon \in [0, \varepsilon_0]$ with $\varepsilon_0 > 0$. Recall that the transition $\bar{\pi}_1 : \bar{\Sigma}_1 \to \bar{\Sigma}_2$ is equivalent to the transition map $\pi_1 : \Sigma_1 \to \Sigma_2$ in the sense that it has the same properties. Furthermore, via the matching maps κ_{ij} defined in Lemma 7, we have appropriately identified the relevant sections in each of the charts, allowing us to follow the flow of the blown-up vector field along the three charts.

As summarized above, the transition map $\bar{\pi}_1 : \bar{\Sigma}_1 \to \bar{\Sigma}_2$ is well-defined for $\varepsilon \in [0, \varepsilon_0]$ and smooth for $\varepsilon \in (0, \varepsilon_0]$ for some $\varepsilon_0 > 0$. It remains to prove that $\bar{\pi}_1$ is a contraction. From Lemma 3 we know that the solutions started in $\bar{\Sigma}_1$ are contracting, see (Fig. 7). This family of orbits is continued to chart K_2 by spending an $O(1)$-time on the time scale t_2 of system (56). This continuation persists (Theorem 4) during the passage near the point q_{e_3} in chart K_3 until it reaches the section $\bar{\Sigma}_2$. As the contraction persists from $\bar{\Sigma}_1$ to $\bar{\Sigma}_2$, one concludes that $\bar{\pi}_1$ is a contraction. This completes the proof. □

4.2. Blow-up of the non-hyperbolic line $\ell_2 \times \{0\}$ and a sketch of the proof of Lemma 5

In this subsection, for the sake of brevity, we summarize the blow-up of the non-hyperbolic line $\ell_2 \times \{0\}$ and give a sketch of the proof of Lemma 5. To this end, we transform the non-hyperbolic line of steady states $\ell_2 \times \{0\}$ by

$$f = \tilde{f}, \qquad c = r\tilde{c}, \qquad \varepsilon = r\tilde{\varepsilon}, \qquad e = r\tilde{e}, \tag{74}$$

where $\tilde{c}^2 + \tilde{e}^2 + \tilde{\varepsilon}^2 = 1$, $\bar{f} \in [0, 1]$ and $r \geq 0$, and define the charts $\tilde{K}_1, \tilde{K}_2$ and $\tilde{K}_3$ as follows

$$\begin{aligned}
\tilde{K}_1 : &\quad f = \tilde{f}_1, &\quad c = \tilde{r}_1\tilde{c}_1, &\quad \varepsilon = \tilde{r}_1\tilde{\varepsilon}_1, &\quad e = \tilde{r}_1,\\
\tilde{K}_2 : &\quad f = \tilde{f}_2, &\quad c = \tilde{r}_2\tilde{c}_2, &\quad \varepsilon = \tilde{r}_2, &\quad e = \tilde{r}_2\tilde{e}_2,\\
\tilde{K}_3 : &\quad f = \tilde{f}_3, &\quad c = \tilde{r}_3, &\quad \varepsilon = \tilde{r}_3\tilde{\varepsilon}_3, &\quad e = \tilde{r}_3\tilde{e}_3.
\end{aligned}$$

$\tilde{K}_1 = \{\tilde{e} = 1\}$

Recall that the goal of Lemma 5 is to describe the map $\pi_2 : \Sigma_2 \to \Sigma_3$ in the original space. In this subsection, we present a sketch of the proof of Lemma 5 by constructing the corresponding map $\bar{\pi}_2 : \bar{\Sigma}_2 \to \bar{\Sigma}_3$

in the blown-up space, and interpreting the results for fixed $\varepsilon \in [0, \varepsilon_0]$ for some $\varepsilon_0 > 0$. For the sake of brevity, we have summarized the analysis of the blow-up of the non-hyperbolic line $\ell_2 \times \{0\}$ in Fig. 16.

First of all, note that the non-hyperbolic line ℓ_2, which is the intersection of the critical manifolds $c = 0$ and $e = 0$, has been blown-up to the orange cylinder (see Fig. 16). We have illustrated the slow flows in the planes $c = 0$ and $e = 0$ in blue. Note that the orbits $\bar{\omega}_7$ and $\bar{\omega}_1$ which are in the blown-up space correspond, respectively, to the orbits ω_7 and ω_1 in the original space (see Figs. 9 and 16). As it is shown in Fig. 16, the intersection of the cylinder with $\bar{\omega}_7$ and $\bar{\omega}_1$ is denoted by $\tilde{p}_f$ and $\tilde{p}^f$, respectively.

Our analysis in chart $\tilde{K}_1$ proves that there exists a three-dimensional attracting center manifold at the point $\tilde{p}_f$, which is the continuation of the family indexed by ε of the attracting slow manifold $\bar{\mathcal{S}}^{\mathrm{a}}_{0,2}$. In view of such a center manifold, the family of the slow manifold $\bar{\mathcal{S}}^{\mathrm{a}}_{0,2}$ enters the chart $\tilde{K}_2$. Our analysis in chart $\tilde{K}_2$ proves that there exists a hyperbolic attracting one-dimensional slow manifold $\tilde{\mathcal{N}}^0$, which attracts the interior of the cylinder. Our analysis in chart $\tilde{K}_3$ shows that the critical manifold $\tilde{\mathcal{N}}^0$ limits at the point $\tilde{p}^f$ (see Fig. 16). Note that $\tilde{p}^f$ is a *degenerate* point, i.e., the linearization of the blown-up dynamics in chart $\tilde{K}_3$ at $\tilde{p}^f$ has a stable eigenvalue, and a triple zero eigenvalues which allows us to construct a three-dimensional attracting center manifold. Therefore the family of flows follows such a center manifold and then intersects the section Σ_3 in a point $(f(\varepsilon), \delta_3, e(\varepsilon))$, for some $\delta_3 > 0$, which is exponentially close to the slow manifold $\mathcal{S}^{\mathrm{a}}_{\varepsilon,3}$ and converges to the point $q_3 := \Sigma_3 \cap \omega_1$ as $\varepsilon \to 0$. This proves that the transition map $\bar{\pi}_2 : \bar{\Sigma}_2 \to \bar{\Sigma}_3$ and hence $\pi_2 : \Sigma_2 \to \Sigma_3$ are well-defined for $\varepsilon \in [0, \varepsilon_0]$ and also are smooth for $\varepsilon \in (0, \varepsilon_0]$, for some $\varepsilon_0 > 0$. The proof of contraction of the transition map π_2 follows the same line of reasoning as that of the map π_1, and hence is omitted for brevity.

5. Conclusions

In this work we have studied a model that describes several important properties of myxobacteria during development [16]. This model, which is in line with observation from experiments [16], acts as an internal clock to control the gliding motions in myxobacteria. When two cells collide with each other, the speed of the clock in both cells is affected, some spatial wave patterns are created, and hence lead to synchronization of cells, i.e., fruiting body. The model presented in [16] can reproduce observed spatial patterns in experiments, and furthermore, it can explain both the cellular oscillations and the developmental stage of myxobacteria from vegetative swarming to the rippling phase and hence to the formation of the fruiting body.

The model, described by a system of three ordinary differential equations, has oscillatory behavior for certain parameter values, and sufficiently small Michaelis-Menten constants which we have unified them by a parameter ε. We have analyzed the dynamics of this oscillator in the limits of ε, and proven that for sufficiently small ε, there exists a strongly attracting limit cycle. The geometric method could be pushed to analyze the global uniqueness of the limit cycle which is clearly of great interest from both the mathematical and biological point of view. This requires a more global analysis of the singular flows, and in particular, connecting orbits between the critical manifolds $\mathcal{S}_{0,i}$ by orbits of the layer problem. As the layer problem is linear, this is possible. Our approach has been based on the geometric perturbation analysis and blow-up method. The geometric perturbation theory and geometric desingularization by several blow-ups allow us to fully understand the structure of the limit cycle. We emphasize that the approach and tools presented in this paper, i.e. geometric singular perturbation theory and the blow-up method, are not limited to the analysis of the system (4); these tools can be applied to similar systems such as [22] whose parameters have the property of zero-order ultrasensitivity.

As discussed in Appendix A, the limit cycle has the same qualitative behavior as the singular cycle provided that $\gamma \in (0.0561, 0.1177)$. From the biological point of view, it is crucial to have γ in a certain range between 0 and 1 as it is the C-signal of the system. The simultaneous limit $(\varepsilon, \gamma) \to (0, 0)$ is very singular because the point $(0, 0, \gamma)$, playing a crucial role in our analysis, approaches $(0, 0, 0)$ which is the intersection of three critical manifolds $f = 0$, $c = 0$, and $e = 0$. Mathematically, it is interesting to study

this limit further, which could explain the coalescence of the Hopf curve and the saddle-node curve at $(0,0)$, see Fig. 4. Similar remark holds as $(\varepsilon,\gamma)\to(0,1)$.

Appendix A. Range of parameter γ in Theorem 2

Although in our analysis we have fixed the parameter $\gamma = 0.08$, in this appendix we show that the behavior of the singular cycle Γ_0, illustrated in Fig. 9, will remain qualitatively the same under a sufficiently small perturbation of γ, and hence Theorem 3.22 holds for these values as well.

As it is shown in Fig. 9, ω_1 and ω_3 are described by the layer problem (18), whose behavior highly depends on parameter γ. For the former, observations from numerical simulations show that if the layer problem starts from a point in $\mathcal{S}^{\rm a}_{0,3}$, namely $p_\gamma := (f_\gamma, \frac{1}{2}, 0) \in \ell_e$ when $\frac{1}{2} < f_\gamma < 1$, the parameter γ can influence the fast dynamics to move from p_γ to a point either in $\mathcal{S}^{\rm a}_{0,1}$, $\mathcal{S}^{\rm a}_{0,2}$, $\mathcal{S}^{\rm a}_{0,3}$, $\mathcal{S}^{\rm a}_{0,4}$, $\mathcal{S}^{\rm a}_{0,5}$ or $\mathcal{S}^{\rm a}_{0,6}$. For the latter, numerical simulations show that if the layer problem starts from a point in $\mathcal{S}^{\rm a}_{0,6}$, namely $p^\gamma := (f^\gamma, \frac{1}{2}, 1) \in \ell^e$ when $0 < f^\gamma < \frac{1}{2}$, the parameter γ can influence the fast dynamics to move from p^γ to a point either in $\mathcal{S}^{\rm a}_{0,1}$ or $\mathcal{S}^{\rm a}_{0,2}$. In this regard, it is interesting to find a certain range for γ such that the qualitative behavior of the fast dynamics remains the same as ω_1 and ω_3, shown in Fig. 9, i.e., the fast dynamics moves *directly* from p_γ to a point in $\mathcal{S}^{\rm a}_{0,6}$, and from p^γ to a point in $\mathcal{S}^{\rm a}_{0,1}$, while does not intersect with the other planes.

In view of equations (27), one can show that the slow flow, started from the point $p^f = (\frac{1}{2}, 0, 0)$, will reach the point $p_1 = (\frac{1+\sqrt{\gamma}}{2}, \frac{1}{2}, 0)$. In order to find a certain range for γ, as the layer problem (18) is linear, one can find the closed form of solutions. In view of the boundary conditions in $\mathcal{S}^{\rm a}_{0,3}$ and $\mathcal{S}^{\rm a}_{0,6}$, we will get a system of transcendental equations, whose solution determines a point at which ω_1 intersects with $\mathcal{S}^{\rm a}_{0,6}$. However, due to the fact that it is impossible to solve such a system of equations analytically, we have used numerical methods to calculate the solution of transcendental equations. Computed numerically, for any $\gamma \in \mathcal{R}_1 := (0.0561,\, 0.1177)$, the qualitative behavior of the fast dynamics is the same as ω_1, illustrated in Fig. 9. Moreover, one can check that for such a range, the qualitative behavior of the fast dynamics is the same as ω_3 as well, illustrated in Fig. 9. Therefore, one concludes that Theorem 2 is valid for all $\gamma \in \mathcal{R}_1$. Analogously, one can find a range for the case that γ is close to 1, see Remark 3.

Appendix B. Line ℓ_c as a fold line

In this appendix, we follow [24, Lemma 6] to show that the line ℓ_c is a fold line except at $f \in \{0, \frac{1}{2}, 1\}$. Similar results hold for lines ℓ_f and ℓ_e, whose analyses are omitted for brevity.

In Section 3.1, we have shown that the layer problem is governed by the equations

$$\begin{aligned}
\frac{df}{d\tau} &= (\gamma - e)\, H^0(f,c,e),\\
\frac{dc}{d\tau} &= 2\,(2f-1)\, H^0(f,c,e),\\
\frac{de}{d\tau} &= 2(2c-1) H^0(f,c,e),
\end{aligned}$$

in which

$$H^0(f,c,e) = 32fce(1-f)(1-c)(1-e).$$

As shown in (18), the fast fibers of the layer problem away from the critical manifold (i.e., when $(f,c,e) \in \mathring{\mathcal{Q}}$) are spanned by the following vector field:

$$V_s(f,c,e) = \begin{pmatrix} \gamma - e \\ 2(2f-1) \\ 2(2c-1) \end{pmatrix}.$$

The first and second derivatives of H^0 and the first derivative of V_s are computed as follows:

$$\mathrm{D}H^0 = \begin{pmatrix} 32ce(1-2f)(1-c)(1-e) & 32fe(1-f)(1-2c)(1-e) & 32fc(1-f)(1-c)(1-2e) \end{pmatrix},$$

$$\mathrm{D}^2H^0 = \begin{pmatrix} -64ce(1-c)(1-e) & 32e(1-2f)(1-2c)(1-e) & 32c(1-2f)(1-c)(1-2e) \\ 32e(1-2f)(1-2c)(1-e) & -64fe(1-f)(1-e) & 32f(1-f)(1-2c)(1-2e) \\ 32c(1-2f)(1-c)(1-2e) & 32f(1-f)(1-2c)(1-2e) & -64fc(1-f)(1-c), \end{pmatrix},$$

$$\mathrm{D}V_s = \begin{pmatrix} 0 & 0 & -1 \\ 2f & 0 & 0 \\ 0 & 4c & 0 \end{pmatrix}.$$

Following [24, Lemma 6 and Section 4.3], we have

$$\mathrm{D}H_0V_s|_{\{e=0\}} = 64fc(c-1)(2c-1)(f-1), \tag{B.1}$$

which indeed shows that $\mathcal{S}_{0,3}$ loses normal hyperbolicity at $f \in \{0,1\}$ and $c \in \left\{0, \frac{1}{2}, 1\right\}$. Now we restrict our analysis to the line ℓ_c and compute

$$(V_s^\top \mathrm{D}^2H_0V_s + \mathrm{D}H_0\mathrm{D}V_sV_s)|_{\ell_c} = -64f(f-1)(2f-1), \tag{B.2}$$

which confirms that the line ℓ_c is a line of "generic folds" except at $f \in \{0, \frac{1}{2}, 1\}$. Since the limit cycle passes sufficiently away from such a point (see Figs. 8, 9 and 16), we do not study the vicinity of $(f,c,e) = (\frac{1}{2}, \frac{1}{2}, 0)$ further. Following [24], one can easily verify that such a point is a "cusp" contact point for $0 < \gamma < 1$.

References

[1] Carmen Chicone, Ordinary Differential Equations with Applications, Springer Science & Business Media, 2006.
[2] Shui-Nee Chow, Chengzhi Li, Duo Wang, Normal Forms and Bifurcation of Planar Vector Fields, Cambridge University Press, 1994.
[3] Kaiser Dale, Multicellular development in myxobacteria, in: Genetics of Bacterial Diversity, Elsevier, 1989, pp. 243–263.
[4] Olivier Decroly, Albert Goldbeter, Birhythmicity, chaos, and other patterns of temporal self-organization in a multiply regulated biochemical system, Proc. Natl. Acad. Sci. 79 (22) (1982) 6917–6921.
[5] Annick Dhooge, Willy Govaerts, Yu A. Kuznetsov, Matcont: a Matlab package for numerical bifurcation analysis of odes, ACM Trans. Math. Softw. 29 (2) (2003) 141–164.
[6] Freddy Dumortier, Robert H. Roussarie, Canard Cycles and Center Manifolds, vol. 577, American Mathematical Soc., 1996.
[7] Neil Fenichel, Geometric singular perturbation theory for ordinary differential equations, J. Differ. Equ. 31 (1) (1979) 53–98.
[8] Albert Goldbeter, A minimal cascade model for the mitotic oscillator involving cyclin and cdc2 kinase, Proc. Natl. Acad. Sci. 88 (20) (1991) 9107–9111.
[9] Albert Goldbeter, Dissipative structures and biological rhythms, Chaos, Interdiscip. J. Nonlinear Sci. 27 (10) (2017) 104612.
[10] Albert Goldbeter, Daniel E. Koshland, Ultrasensitivity in biochemical systems controlled by covalent modification. Interplay between zero-order and multistep effects, J. Biol. Chem. 259 (23) (1984) 14441–14447.
[11] Albert Goldbeter, John J. Tyson, Biochemical oscillations and cellular rhythms: the molecular bases of periodic and chaotic behaviour, Nature 380 (6571) (1996) 213–214.
[12] Brian C. Goodwin, Oscillatory behavior in enzymatic control processes, Adv. Enzyme Regul. 3 (1965) 425.
[13] John Guckenheimer, Philip J. Holmes, Nonlinear Oscillations, Dynamical Systems, and Bifurcations of Vector Fields, vol. 42, Springer Science & Business Media, 2013.
[14] Ilona Gucwa, Peter Szmolyan, Geometric singular perturbation analysis of an autocatalator model, Discrete Contin. Dyn. Syst., Ser. S 2 (2009) 783–806.
[15] Alan L. Hodgkin, Andrew F. Huxley, A quantitative description of membrane current and its application to conduction and excitation in nerve, J. Physiol. 117 (4) (1952) 500–544.
[16] Oleg A. Igoshin, Albert Goldbeter, Dale Kaiser, George Oster, A biochemical oscillator explains several aspects of myxococcus xanthus behavior during development, Proc. Natl. Acad. Sci. USA 101 (44) (2004) 15760–15765.
[17] Hildeberto Jardón-Kojakhmetov, Christian Kuehn, A survey on the blow-up method for fast-slow systems, arXiv preprint arXiv:1901.01402, 2019.
[18] Ilona Kosiuk, Relaxation oscillations in slow-fast systems beyond the standard form, PhD thesis, Univ. Leipzig, 2012.
[19] Ilona Kosiuk, Peter Szmolyan, Geometric analysis of the goldbeter minimal model for the embryonic cell cycle, J. Math. Biol. 72 (5) (2016) 1337–1368.

[20] Martin Krupa, Peter Szmolyan, Extending geometric singular perturbation theory to nonhyperbolic points—fold and canard points in two dimensions, SIAM J. Math. Anal. 33 (2) (2001) 286–314.
[21] Christian Kuehn, Multiple Time Scale Dynamics, vol. 191, Springer, 2015.
[22] Carmen Kut, Vahid Golkhou, Joel S. Bader, Analytical approximations for the amplitude and period of a relaxation oscillator, BMC Syst. Biol. 3 (1) (2009) 6.
[23] Yuri A. Kuznetsov, Elements of Applied Bifurcation Theory, vol. 112, Springer Science & Business Media, 2013.
[24] Ian Lizarraga, Robert Marangell, Martin Wechselberger, Slow unfoldings of contact singularities in singularly perturbed systems beyond the standard form, J. Nonlinear Sci. (2020) 1–38.
[25] Béla Novák, John J. Tyson, Design principles of biochemical oscillators, Nat. Rev. Mol. Cell Biol. 9 (12) (2008) 981–991.
[26] Peter Szmolyan, Martin Wechselberger, Relaxation oscillations in $\mathbb{R}^3$, J. Differ. Equ. 200 (1) (2004) 69–104.
[27] Hadi Taghvafard, Modeling, Analysis, and Control of Biological Oscillators, PhD thesis, University of Groningen, 2018.
[28] Hadi Taghvafard, Hildeberto Jardón-Kojakhmetov, Ming Cao, Parameter-robustness analysis for a biochemical oscillator model describing the social-behaviour transition phase of myxobacteria, Proc. R. Soc. A 474 (2209) (2018) 20170499.
[29] Hadi Taghvafard, Anton V. Proskurnikov, Ming Cao, Local and global analysis of endocrine regulation as a non-cyclic feedback system, Automatica 91 (2018) 190–196.
[30] Hadi Taghvafard, Alexander Medvedev, Anton V. Proskurnikov, Ming Cao, Impulsive model of endocrine regulation with a local continuous feedback, Math. Biosci. 310 (2019) 128–135.
[31] Balth van der Pol, Jan van der Mark, The heartbeat considered as a relaxation oscillation, and an electrical model of the heart, Philos. Mag. 6 (38) (1928) 763–775.
[32] Martin Wechselberger, Geometric Singular Perturbation Theory Beyond the Standard Form, Springer, 2020.
[33] Arthur T. Winfree, Biological rhythms and the behavior of populations of coupled oscillators, J. Theor. Biol. 16 (1) (1967) 15–42.